Cell Reports

Article

MetA is a "thermal fuse" that inhibits growth and protects *Escherichia coli* at elevated temperatures

Graphical abstract

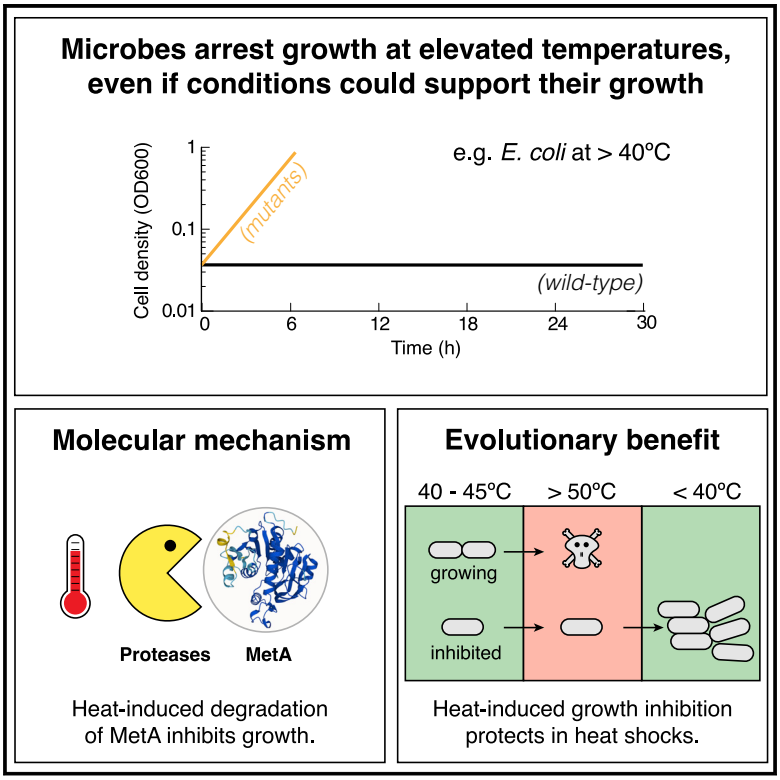

Highlights

- Bacteria possess a fuse that protects them from dying at high temperatures
- The fuse is an induced methionine-auxotrophy that causes growth inhibition
- Growth-inhibited bacteria survive heat shocks 1,000-fold better than growing bacteria

Authors

Severin J. Schink, Zara Gough, Elena Biselli, Mariel Garcia Huiman, Yu-Fang Chang, Markus Basan, Ulrich Gerland

Correspondence

info@severin-schink.eu (S.J.S.), gerland@tum.de (U.G.)

In brief

Schink et al. report that at high temperatures, bacteria cut off their methionine production, which halts biosynthesis and growth, similar to how a thermal fuse cuts off electricity in electrical devices. The resulting growth arrest protects bacteria should temperatures further rise beyond the habitable range.

Schink et al., 2022, Cell Reports *40*, 111290
August 30, 2022
https://doi.org/10.1016/j.celrep.2022.111290

CellPress

Cell Reports

CellPress
OPEN ACCESS

Article

MetA is a "thermal fuse" that inhibits growth and protects *Escherichia coli* at elevated temperatures

Severin J. Schink,[1,2,3,*] Zara Gough,[2,3] Elena Biselli,[2,3] Mariel Garcia Huiman,[2] Yu-Fang Chang,[1] Markus Basan,[1] and Ulrich Gerland[2,4,*]

[1]Department of Systems Biology, Harvard Medical School, 200 Longwood Avenue, Boston, MA 02115, USA
[2]Physics of Complex Biosystems, Physics Department, Technical University of Munich, 85748 Garching, Germany
[3]These authors contributed equally
[4]Lead contact
*Correspondence: info@severin-schink.eu (S.J.S.), gerland@tum.de (U.G.)
https://doi.org/10.1016/j.celrep.2022.111290

SUMMARY

Adaptive stress resistance in microbes is mostly attributed to the expression of stress response genes, including heat-shock proteins. Here, we report a response of *E. coli* to heat stress caused by degradation of an enzyme in the methionine biosynthesis pathway (MetA). While MetA degradation can inhibit growth, which by itself is detrimental for fitness, we show that it directly benefits survival at temperatures exceeding 50°C, increasing survival chances by more than 1,000-fold. Using both experiments and mathematical modeling, we show quantitatively how protein expression, degradation rates, and environmental stressors cause long-term growth inhibition in otherwise habitable conditions. Because growth inhibition can be abolished with simple mutations, namely point mutations of MetA and protease knockouts, we interpret the breakdown of methionine synthesis as a system that has evolved to halt growth at high temperatures, analogous to "thermal fuses" in engineering that shut off electricity to prevent overheating.

INTRODUCTION

Microbes in nature face a variety of environments, ranging from ideal growth conditions to hostile environments, where stressors threaten their survival. One such stressor is elevated temperature, which can arise quickly and unpredictably. When temperatures rise above the optimal range, microbes employ a well-characterized heat-shock response (Yura and Nakahigashi, 1999; Arsène et al., 2000; Richter et al., 2010). Molecular chaperones protect proteins in the cytoplasm and periplasm by maintaining their native conformation (Bukau, 1993; Yura and Nakahigashi, 1999; Arsène et al., 2000), and proteases degrade misfolded and aggregated proteins (Laskowska et al., 1996). DNA repair is upregulated (Nonaka et al., 2006) and toxic reactive oxygen species, which are at particularly high levels at elevated temperatures (Marcén et al., 2017), are scavenged by catalases (Mackey and Seymour, 1987), superoxide dismutases (Privalle and Fridovich, 1987), and small molecules such as glutathione (Laman Trip and Youk, 2020; Marcén et al., 2019). The induction of these protective genes, collectively referred to as the heat-shock response, permits cells to maintain their functionality and recover once conditions have improved.

However, some responses of microbes appear less logical. A long-standing puzzle is the active degradation of a key enzyme in the methionine biosynthesis pathway, homoserine *O*-succinyltransferase (MetA), when temperatures increase (Ron and Shani, 1971; Biran et al., 1995, 2000). This degradation causes methionine limitation, which slows the growth of cultures not supplemented with methionine (Gur et al., 2002; Ron and Davis, 1971a) and decreases the maximum growth temperature in minimal medium from 47°C to 45°C (Mordukhova et al., 2008). The degradation of MetA was found across bacterial species from Enterobacteriaceae, including *Escherichia coli*, *Salmonella typhimurium*, and *Klebsiella aerogenes* (Ron, 1975) to Alphaproteobacteria such as *Agrobacterium fabrum* (Rotem et al., 2013). Even in the Gram-positive *Paenibacillus polymyxa* (Wyman et al., 1975) and *Corynebacterium glutamicum* (Hwang et al., 2002), in which MetA and MetXA, respectively, encode a homoserine *o*-acetyltransferase rather than an *o*-succinyltransferase, the temperature-dependent degradation is conserved. This conservation is conspicuous because MetA is only weakly conserved between these species (Figure S1), but is the only biosynthetic enzyme that is degraded at high rates (>1/h) (Biran et al., 1995) compared with the rest of the proteome (0.2–0.01/h) (Maurizi, 1992). Furthermore, MetA degradation is not inevitable, since several point mutations were discovered that decrease degradation rates, alleviate growth defects, and increase the maximum growth temperature (Mordukhova et al., 2008, 2013). Ron and coworkers hypothesized that MetA could serve as a regulatory protein (Biran et al., 2000; Gur et al., 2002; Ron, 1975), given that it displays rapid ATP-dependent proteolysis in combination with activation of transcription

(Biran et al., 1995, 2000), a hallmark of regulatory proteins that enable quick response times (Gottesman and Maurizi, 1992). However, it is unclear why stalling methionine biosynthesis should be actively regulated by bacteria, because there would need to be "some undisclosed selective benefit," as stated by Ron and Davis (1971a). To date, the only described benefit is an increase in antibiotic persistence at elevated temperatures, discovered by Mordukhova and Pan (2014), but there is no apparent relation between antibiotic stress and heat stress.

Here, we identify the missing selective benefit of MetA degradation. Furthermore, we confirm the hypothesis that MetA dually serves as a biosynthetic protein and a temperature-sensitive regulatory protein, and clarify the mechanism whereby MetA controls growth at elevated temperatures. Using *E. coli* as a model system, we show that MetA plays a central role in this regulated growth inhibition that protects from cell death when temperature is further increased. The protective effect of growth inhibition against heat shocks appears to be a general physiological feature of microbes, as we can reproduce the phenomenon in *Saccharomyces cerevisiae*. Hence, heat-induced growth inhibition appears to implement a "heat-induced persistence" strategy that is conceptually similar to antibiotic persistence (Balaban et al., 2004; Harms et al., 2016) and modulated by MetA degradation.

RESULTS

Elevated temperatures induce growth inhibition in *E. coli*

To probe how heat affects the physiology of bacteria, we exposed cultures of *E. coli* K-12 grown in minimal medium at elevated temperatures to a period of carbon starvation, such that cells could accumulate damage in the absence of nutrients required for essential maintenance. Owing to the absence of nutrients required for *de novo* synthesis, this period reveals the deteriorative effects of temperature on the cell. After the starvation period, we reinoculated the culture in fresh minimal medium with a carbon substrate and observed the resulting recovery of the stressed culture. The temperature was kept constant throughout the entire experiment, i.e., initial growth, starvation, and recovery. We observed that the regrowth during the recovery phase displays lag times that depend on temperature (Figure 1A). At 37°C, cultures recovered quickly, while at 45°C, the maximum growth temperature, the culture required more than 10 h to recover. Such long recovery times at high temperatures are puzzling because the majority of bacteria remain viable during the recovery, as assayed by plating on lysogeny broth (LB) agar at 37°C (Figure S2), implying that the long lag times are not due to cell death but are instead caused by viable bacteria not growing.

The lag time also increases with the prior starvation duration (Figure 1B), suggesting that cells gradually lose the ability to grow. For 1 h of starvation, cultures recovered within 2 h, but if starvation took longer than 9 h at 45°C, cultures did not recover within the 3 days of the experiment.

There are two qualitatively different scenarios for how long lag times may arise. One scenario is a homogeneous population of cells that all require a similarly long time to recover. The other scenario has two subpopulations; a large non-growing population and a small growing population. In the second case, the lag time is given by the time it takes for the small, growing population to dominate the cell count. To distinguish between these scenarios, we assayed the recovery phase at the single-cell level: we extracted samples of a starved culture at 45°C and deposited them on pre-warmed agar pads supplemented with carbon substrate to allow recovery. We stained the bacteria with propidium iodide (red) for membrane permeability to detect cell death, and monitored growth by time-lapse microscopy (see STAR Methods). Figure 1C shows two snapshots from a time lapse, 2 h and 8 h after nutrient addition: The culture, previously starved for 3 h, shows three distinct populations. Five percent of the population stains positive for cell permeability and are likely dead. A second, small subpopulation (2%), recovered after about 2 h and, after 8 h, has formed microcolonies, which are visible in Figure 1C (white arrowhead). The third and major subpopulation, 93%, stained negative for cell permeability but did not grow within the 12 h of this time lapse. These data show that recovery is highly heterogeneous; few cells recover early and dominate the recovery.

In an experimental scenario similar to ours, Laman Trip and Youk (2020) recently observed that *S. cerevisiae* arrest growth when cultures are diluted during exponential growth at elevated temperatures. Indeed, this density-dependent growth behavior is shared by *E. coli*: we found that if cultures are diluted during exponential growth, their growth is also inhibited (Figure S3A). The fact that both yeast and bacteria arrest growth in various different scenarios at high temperature poses an interesting possibility that heat-induced growth inhibition is a more general hallmark of microbes, and triggers the question: is there a fitness benefit to heat-induced growth inhibition?

Growth inhibition protects *E. coli* from heat shocks

Because growth inhibition is observed at temperatures close to the growth limit (40°C–45°C for *E. coli*), but in a regime where conditions still eventually allow growth, we wondered whether growth inhibition is an evolutionarily "chosen" strategy rather than an accident. For such a strategy to evolve there would need to be a selective benefit associated with growth inhibition, which outweighs the cost of reduced growth. To examine possible selective benefits, we exposed *E. coli* cultures to sudden heat shocks. We used our standard starvation protocol (Figures 1A–1C) to induce growth inhibition, using a 5-h period of starvation and subsequent reinoculation in fresh medium at 44°C. We took samples from the culture every hour after reinoculation, heat shocked them for 10 min at 52°C, and measured the resulting viability. Strikingly, growth-inhibited cultures survived heat shocks almost unscathed, while in cultures heat shocked in exponential growth, only about 0.7% survived (Figure 1D). The existence of this benefit shows that growth inhibition could in principle be used by microorganisms as part of the response to heat stress. To investigate this possibility, we next sought to understand what causes growth inhibition in *E. coli*.

Breakdown of methionine synthesis causes growth inhibition in *E. coli*

It is known that high temperature leads to denaturation of the proteome (Dill et al., 2011; Leuenberger et al., 2017). One protein,

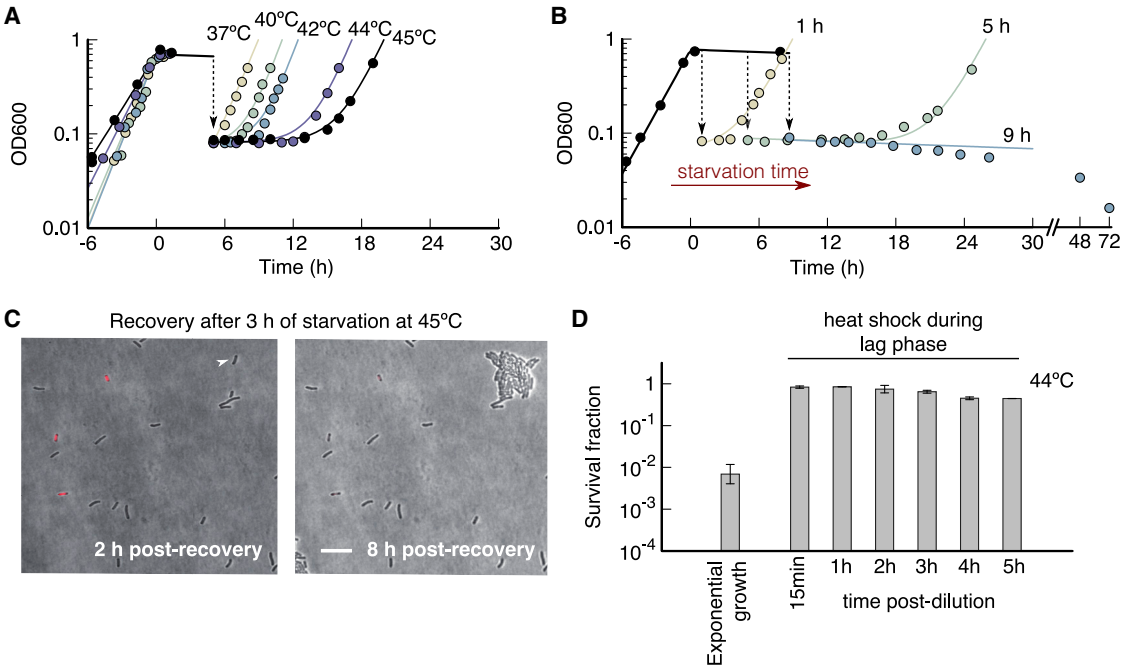

Figure 1. Starvation at elevated temperatures induces growth inhibition

(A) Optical density OD_{600} of *Escherichia coli* K-12 grown until nutrient depletion, first starved for 5 h, then diluted into fresh medium to allow recovery. Colors denote culture temperatures, kept constant throughout each experiment. Lag times of cultures increase with temperature, from ~23 min at 37°C, to 11.1 h at 45°C. In (A) to (C), growth is fitted as exponential $N(t) = N(0)e^{\mu t}$ and recovery as a combination of decay and growth $N(t) = N_1e^{-\gamma t} + N_2e^{\mu t}$, with $\gamma = 0.1\ h^{-1}$. Lag times are extracted as detailed in STAR Methods. Data show results from single experiments.

(B) Lag times at 45°C increase with starvation duration. No recovery was recorded within 3 days for 9 h starvation (blue) or longer. Data are from single experiments.

(C) Snapshots of time-lapse movies during recovery at 45°C on glycerol minimal medium agar pads (see STAR Methods). Fluorescence of propidium iodide (red) reports permeability. One growing cell (white arrowhead) grows to a microcolony after 8 h of incubation. Scale bar, 10 μm.

(D) Killing by heat shock (52°C, 10 min) of *E. coli* cultured at 44°C in exponential growth (white) or during lag phase after 5 h of starvation and dilution (gray). *E. coli* growth arrested during lag phase is completely protected from heat killing at 52°C. The survival fraction was measured by plating on LB agar at 37°C before and after the heat shock. Bars show mean of three biological repeats, and error bars show standard deviation.

homoserine O-succinyltransferase (MetA), which catalyzes the first commitment step of the methionine biosynthesis pathway, is particularly susceptible to heat stress (Ron and Davis, 1971a; Biran et al., 1995, 2000). This enzyme aggregates and is degraded (Gur et al., 2002). The resulting methionine limitation leads to a decrease in growth rate compared with cultures supplemented with methionine at elevated temperatures and completely arrests growth above 45°C (Figure S4). Cultures supplemented with methionine in turn were able to grow up to 47°C.

To test whether the long lag times are due to methionine limitation, we supplemented the regrowth medium with methionine and found a drastic reduction in lag time, from over 10 h without methionine down to less than 30 min with methionine (Figure 2A). Similarly, performing the experiment in rich medium (LB) instead of minimal medium led to immediate recovery after starvation at 45°C (Figure S5). Growth arrest induced by dilution was also alleviated by the presence of methionine, decreasing the minimum initial population density from which cultures could regrow by 100-fold (Figure S5). Investigating lag times on a single-cell level, we found that if the agar pad was supplemented with methionine, the majority of the cells recovered after starvation (63% compared with 2% without methionine), while the growth-arrested and non-permeable subpopulation virtually disappeared (5% compared with 93% without methionine) (Figure 2B). The absence of the growth-arrested subpopulation (Figure 2B) is consistent with the drastic reduction in lag times observed in bulk measurements (Figure 2A).

To test whether methionine limitation is due to MetA degradation and not a different enzyme in the methionine pathway, we tested MetA mutants with reduced degradation rates, either due to a single-point mutation (I124L) or three-point mutations (I124L-I229Y-N267D, denoted as LYD) identified by Mordukhova et al. (2013). Indeed, these mutants, which have 2- to 3-fold decreased degradation rates (Mordukhova et al., 2013), showed a significant decrease in lag times from about 11 h to about 5 h for the single-point mutant (I124L) and 4 h for the triple-point mutant (LYD) (Figure 2C).

Following these experiments, we wondered whether a period of starvation was necessary to induce growth inhibition or whether it may also be observed directly following a state of exponential growth. To test this, cultures growing exponentially at 42°C in minimal medium supplemented with or without methionine were upshifted to 45°C. We observed that in the presence of methionine cultures continued to grow following the transfer, whereas growth

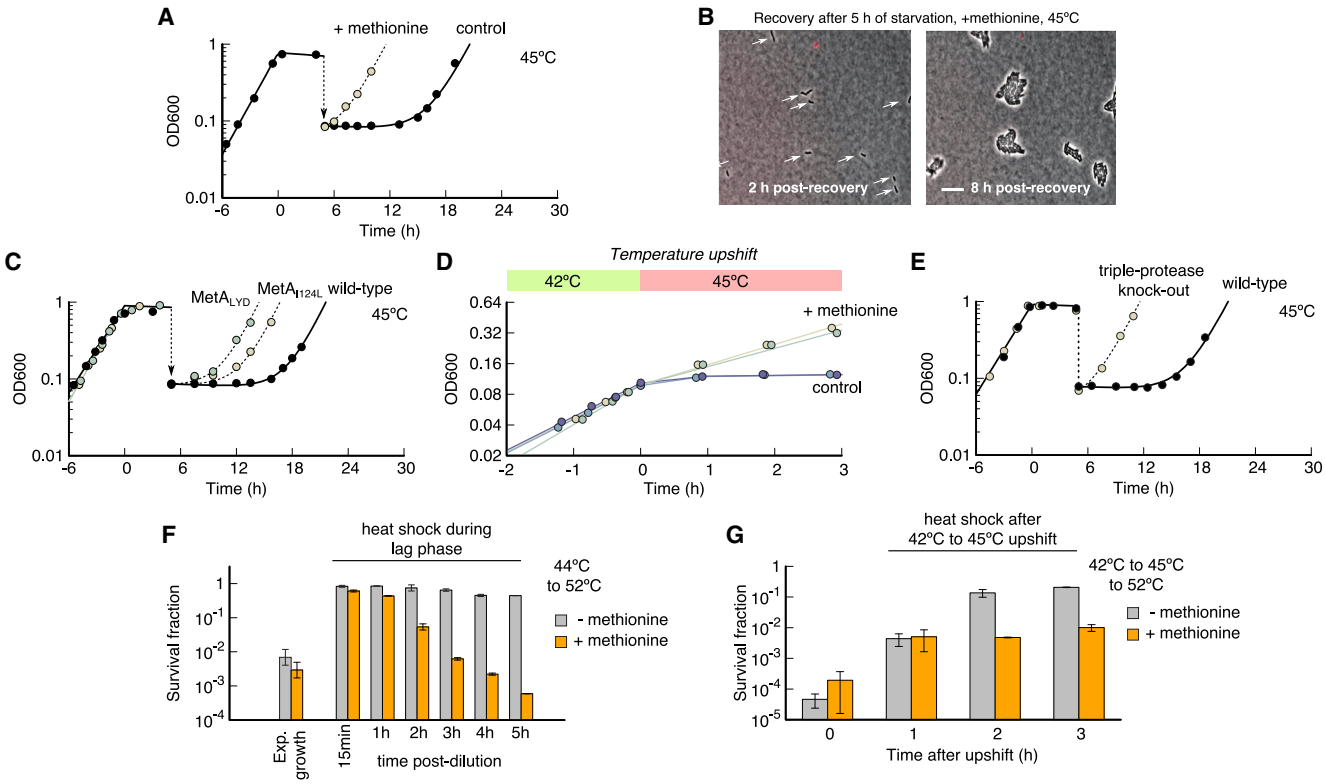

Figure 2. Growth-inhibited cells are methionine limited due to MetA degradation and are protected in heat shocks

(A) Cultures supplemented with methionine recover quickly. Lag times (45°C, 5 h starvation) in cultures supplemented with methionine during regrowth are more than 90% shorter than without methionine (T_{lag} = (0.64 ± 0.02) h compared with T_{lag} = (11.08 ± 0.4) h, n = 2 biological repeats, p < 0.001).

(B) Snapshots of time lapse of recovery on glycerol agar pads supplemented with methionine. Cells indicated by white arrows recover and form microcolonies after 8 h. Scale bar, 10 μm.

(C) Comparison of wild-type MetA with two thermostable mutants. Lag times (45°C, 5 h starvation) decrease in mutants MetA I124Y (T_{lag} = (5.2 ± 1.0) h, n = 3 biological repeats, p < 0.001) and LYD (T_{lag} = (3.7 ± 0.9) h, n = 3 biological repeats, p < 0.001) compared with wild type (T_{lag} = (11.1 ± 0.3) h, n = 3 biological repeats).

(D) Growth of wild-type *E. coli* during a sudden upshift of temperature from 42°C to 45°C. Cultures supplemented with methionine continued to grow (green and yellow) while cultures without methionine became growth arrested (blue and purple). Data points show individual repeats.

(E) Comparison of wild-type *E. coli* with a triple-protease knockout (*Δlon*, *ΔhslV*, and *ΔclpP*). Absence of protease activity decreases lag time (T_{lag} = (1.1 ± 0.3) h, n = 3 biological repeats, p = 0.0012) compared with wild type (T_{lag} = (10.4 ± 1.6) h, n = 3 biological repeats).

(F) Heat shocks (10 min at 52°C) during exponential growth and during lag times at 44°C in cultures supplemented with and without methionine throughout the experiment. Decrease of viability of the methionine-supplemented culture coincides with growth (prior to killing: at 2 h, 2-fold increase of CFU/mL; at 5 h, 20-fold increase of CFU/mL). The survival fraction was measured by plating on LB agar at 37°C before and after the heat shock. See Figure S2 for absolute quantification of viability. Bars show mean of three biological repeats, and error bars show standard deviation.

(G) Heat shocks (same protocol as for F) after the temperature upshift of (D). Time after upshift refers to the shift from 42°C to 45°C. Bars show the average of two biological repeats, and error bars show the standard deviation.

was inhibited in cultures without methionine (Figure 2D). This result, combined with the growth arrest induced by dilution (Figure S3) and growth arrest at 46°C and 47°C (Figure S4), both during exponential growth, show that the induction of growth arrest is not unique to our lag time protocol but is a general phenomenon in the regime close to the maximum permissive growth temperature.

When we hypothesize growth inhibition to be a response to heat stress, an important question is whether MetA is degraded because it is broken, e.g., aggregated or otherwise damaged, or whether MetA is degraded despite being still functional. The latter option would speak for growth inhibition being a "self-inflicted injury" rather than an accident. To distinguish these two possibilities, we constructed a triple knockout of proteases Δ*lon*, *ΔhslV*, and Δ*clpP*, incapable of degrading cytoplasmic proteins, including MetA (Biran et al., 2000). If these proteases exclusively degrade MetA that is already broken, lag times of the triple-protease knockout mutant should either remain unchanged or even increase due to a buildup of non-degradable protein aggregates. On the other hand, if the proteases *lon*, *hslV*, and *clpP* also degrade MetA that is either functional or can regain function (e.g., by refolding into its native state), lag times should decrease in the Δ*lon ΔhslV* Δ*clpP* mutant due to the higher concentration of active MetA within the cells. In the experiment, we found a striking decrease of lag time from 10 h in wild type down to 1 h in the triple-protease knockout (Figure 2E), showing that methionine limitation is caused by degradation of MetA that is either functional

or may become functional in the future. This means that the methionine limitation is brought upon the cell by itself rather than being caused exclusively by stressors.

If growth inhibition protects *E. coli* during heat shocks and growth inhibition is in turn due to methionine limitation, then the addition of methionine should render cells susceptible to heat again. We tested this hypothesis by heat shocking growth-inhibited cultures at 52°C. Growth inhibition was induced by either starvation or temperature upshifts following exponential growth, with and without methionine (see Figures 2A and 2D for growth dynamics and Figures 2F and 2G for viability after heat shocks). While cultures without methionine were protected for several hours from heat (gray), cultures with methionine (orange) lost up to 99.9% of their viability soon after reinoculation in fresh medium (Figure 2F) or temperature upshift (Figure 2G), confirming that the fitness benefit is methionine dependent.

Metabolic bistability leads to stable growth inhibition

How does methionine limitation trap cells in a state of growth inhibition? This is particularly important in order to understand which mechanisms microbes could use to manipulate the fraction of cells entering growth arrest depending on external conditions. While it is clear that degradation of MetA is detrimental for growth, it is important to note how stable growth inhibition is: entire cultures can remain growth-inhibited for several days, although the conditions would allow for growth if methionine was present (Figures 2 and S2). This stability of growth inhibition is puzzling because one would expect that any residual amount of MetA activity, or import of methionine from perished cells, would kick-start growth by supplying methionine, which in turn would be used to synthesize MetA in a self-enhancing positive feedback loop. To answer these questions, we designed a mathematical model of metabolism and protein synthesis that describes the dynamics of internal methionine concentration c_{met} and the relative abundance (proteome fraction) of MetA, φ_{MetA}. We will use the model to derive a theoretical prediction of lag time and to perform quantitative tests of our hypotheses.

The model, summarized in Figure 3A, incorporates processes that affect the cellular methionine level (solid lines) and the MetA protein relative abundance (dashed lines). Within this model, growth is limited by methionine (Equation 1 in Figure 3A), and MetA is degraded at rate γ, diluted by growth and synthesized together with biomass at rate μ (Equation 2 in Figure 3A). This modeling choice focuses on functional, soluble MetA and absorbs the formation of insoluble MetA aggregates and degradation into a single step. Methionine can either be produced by MetA or taken up from the environment, and is used for protein synthesis and to synthesize *S*-adenosylmethionine (SAM), the major methyl donor of the cell (Equation 3 in Figure 3A). While much of this SAM is recycled back to methionine in the SAM cycle (Figure S6), a significant part is used for biosynthesis of polyamines (Table S2), such as spermine and spermidine, which are important for survival in stress conditions (Jung and Kim, 2003; Khan et al., 1992; Shah and Swiatlo, 2008). We account for polyamine synthesis and other potential losses of methionine flux in a drainage flux (Figure 3A). In the method details section of STAR Methods we show a detailed derivation of the model, and in Table S2 we estimate model parameters based on published measurements.

The recovery dynamics of the methionine-MetA model depends on the degradation rate of MetA (Figure 3B): at low degradation rate all cells, regardless of their initial state, recover to growth (top panel, green trajectories), while at high degradation rate none of the cells recover (bottom panel, red trajectories). In between these two extremes, the population splits depending on the initial relative MetA abundance (Figure 3B, middle panel). Cells above a certain "recovery threshold" accumulate MetA and start growing, while cells below the threshold do not. Because both growth and growth arrest are stable states, this intermediate regime is bistable, and a population can contain cells that are growing and others that are not, a state we refer to as "growth inhibition." Because of the positive-feedback motif between methionine and MetA, the bistability requires a non-linearity in flux (Strogatz, 2018), which in our model is caused by the drain of methionine and disappears if either the drain is shut off (Figure S7A) or if methionine is supplemented in the medium (Figure S7B).

Because whether an individual cell recovers or stays arrested depends on its initial relative MetA abundance, we suspect that fluctuations in relative MetA abundance cause the split of the population. Protein abundance is indeed highly variable among individual bacteria due to the stochasticity of transcription and translation (Friedman et al., 2006; Taniguchi et al., 2010), with a typical standard deviation of 40% (Taniguchi et al., 2010). We thus hypothesize that during growth, the vast majority of cells will lie above the recovery threshold (Figure 3C), and that only due to starvation at elevated temperatures, where MetA will be degraded but not synthesized, the relative abundance distribution will shift to lower values and many cells will fall below the threshold (Figure 3D). As a result, only the exponential tail of the relative MetA abundance distribution will remain above the recovery threshold, leading to a small population of recovering cells. According to the model, the characteristic long lag times observed in Figure 1 emerge from this mixture of growing and non-growing cells (Figure 3E).

The model predicts (STAR Methods) how lag time depends on the fraction of recovering cells and how degradation of MetA reduces the fraction of recovering cells. We find a simple exponential dependence between lag time T_{lag} and the starvation time τ and degradation rate η,

$$T_{lag} \propto \overline{\varphi}_{MetA}^{-1} \exp(\eta\tau), \qquad \text{(Equation 4)}$$

which originates from the exponential tail of relative MetA abundance, caused by the stochasticity of transcription and translation processes ($\overline{\varphi}_{MetA}$ denotes the mean relative MetA abundance). For this approximation, we neglected the single-cell contribution to lag time that stems from the recovery of relative MetA abundance and approximated the tail of a gamma distribution with a simple exponential decay. For this latter reason, the approximation of Equation 4 does not reach zero for $\tau \to 0$, but the full model does (see supplemental information). The exponential dependence is therefore only a valid approximation when lag times are long and dominated by a subpopulation of growing bacteria.

A key prediction from the model in Equation (4) is that the lag time T_{lag} should increase exponentially with starvation time τ. Because lag time in the model is set by the fraction of the

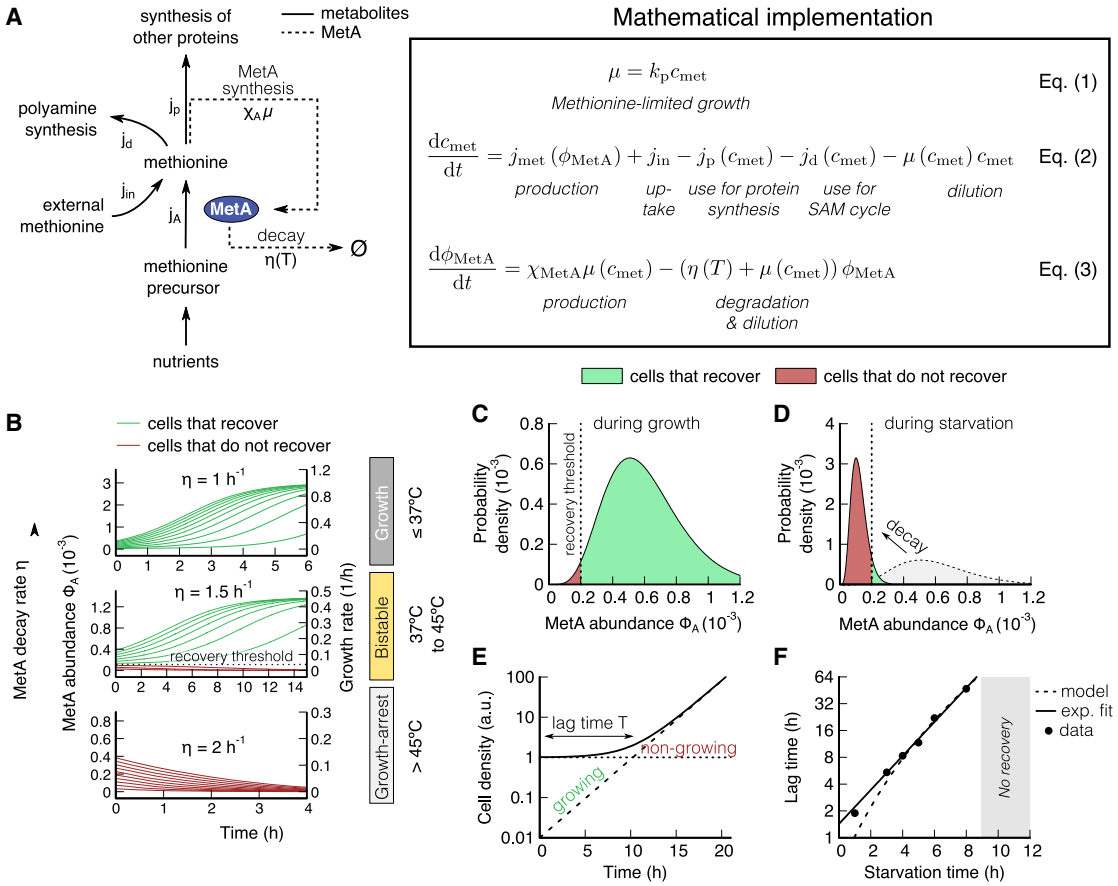

Figure 3. Methionine-MetA model shows that bistability arises from dual use of methionine

(A) Cartoon of the methionine-MetA model. Metabolites: nutrients are taken up, converted first to precursors, and finally to methionine by MetA (blue). See Figure S6 for a detailed methionine biosynthesis pathway. External methionine can be imported if present in the medium. Two fluxes drain methionine, protein synthesis and polyamine synthesis. Proteins: MetA (blue) is synthesized if methionine is present, and will in turn synthesize methionine (positive feedback loop). MetA is degraded at a temperature-dependent rate.

(B) Numerical results of the dynamics of the methionine-MetA model for three different MetA degradation rates (1.0/h, 1.5/h, and 2/h). Whether cells can recover depends on the temperature-dependent degradation rate. At intermediate temperatures (middle panel), we observe that only cells with an initial relative MetA abundance above a recovery threshold can recover (bistable regime).

(C and D) Distribution of relative MetA abundance during growth (C) and starvation (D). Green and red areas indicate cells with relative MetA abundance that allow (green) and do not allow (red) growth.

(E) Recovery dynamics of a mixed culture in batch. The time it takes for the growing fraction to overgrow the non-growing fraction is the lag time.

(F) Theoretical prediction (fit to data of $\tau > 2$ h: dashed line) of lag times compared with experiments (45°C, symbols show individual experiments). Lag time increases exponentially with starvation time $T_{lag} = (1.6 \pm 0.3)\exp(\tau\,(0.43 \pm 0.02)\ \mathrm{h}^{-1})$, fit to all data: solid line. When cultures are starved for more than 9 h, they did not recover within 3 days. The exponential rate fitted, $\eta = (0.43 \pm 0.02)\ \mathrm{h}^{-1}$, is lower than the *in vitro* MetA decay rate of 1.6 h^{-1} measured in Mordukhova et al. (2013), possibly due to low levels of ATP that are required for active degradation during starvation (Biran et al., 2000).

population that recovers, this dependence gives us a direct test of what determines how many cells get trapped in the growth arrest state. Indeed, we can verify the exponential scaling law, and find that it holds a striking >50-fold range in lag times (Figure 3F). Cultures starved for more than 9 h did not recover within 3 days, presumably because all cells of the population are trapped in the growth-arrested state.

The MetA mutants with reduced degradation rates give us the opportunity to test how evolution can tune the fraction of growth-arrested cells, and hence the lag time. The single-point mutant I124L has an experimentally measured degradation rate reduced by 48% compared with wild type (Mordukhova et al., 2013). Using the fit of Equation (4) to the data in Figure 3F, we predict that this 48% reduction in degradation rate should result in a lag time of $T_{lag} = (4.5 \pm 1.0)$ h following a 5-h period of starvation, which matches the observed (5.2 ± 1.0) h of the mutant well (Figure 2C).

In addition, the model can also explain, at least qualitatively, why temperature upshifts (Figure 2D) can lead to growth arrest. If relative MetA abundance inherited from the pre-shift condition at 42°C lies below the recovery threshold, the bacteria will stop growing. This could be due to a number of causes, such as temperature-dependent MetA expression or a higher degradation rate (see supplemental information for details). Degradation rates

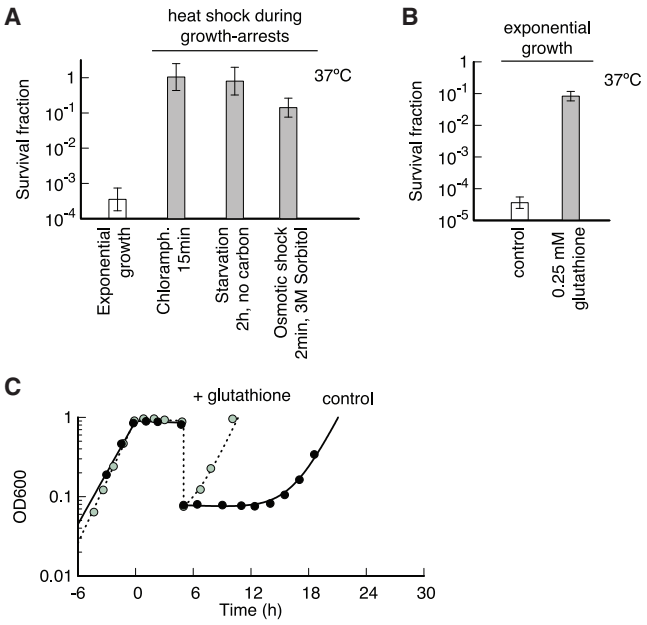

Figure 4. Oxidative stress at elevated temperatures

(A) Killing by heat shock (50°C, 10 min) of *E. coli* cultured at 37°C either in exponential growth (white) or in growth arrest caused by translation inhibition (chloramphenicol), carbon starvation, or hyperosmotic shock (gray). Protection from heat killing is independent of the cause of growth arrest. Bars show average of three biological repeats, with error bars showing standard deviation.

(B) Addition of the antioxidant glutathione rescues heat-induced death (50°C, 10 min) in exponential growth, indicating that oxidative damage is involved at heat-induced death. Bars show average of three biological repeats, with error bars showing standard deviation.

(C) Addition of glutathione reduces lag times after 5 h of starvation from T_{lag} = (1.4 ± 0.2) h to T_{lag} = (10.3 ± 1.6) h, n = 3 biological replicates, p = 0.0013.

could be affected because, for instance, cells are not adapted to high temperatures, e.g., missing heat-shock proteins that can stabilize misfolded proteins. Because we are missing this information, we cannot integrate the temperature-upshift experiment quantitatively into our model, but the observed growth arrest fits well into our understanding of growth as a bistable system.

Growth inhibition protects cells irrespective of cause

Finally, it is still unclear how heat-induced growth inhibition protects cells from subsequent heat shocks. One possibility is that heat-shock proteins, expressed during growth inhibition, prepare cells for the upcoming heat shock. To test this hypothesis, we blocked translation during exponential growth by adding chloramphenicol, which leads to growth arrest without new proteins being synthesized (Nierhaus and Nierhaus, 1973). These experiments were performed at 37°C, when cells are particularly susceptible to subsequent heat shocks. Remarkably, cultures arrested with chloramphenicol survived heat shocks without a significant decrease in viability, whereas the viability of untreated cultures in exponential growth decreased by more than 99.9% (Figure 4A). Growth arrest by inhibition of protein synthesis thus phenocopies the effect of methionine-limited growth inhibition (Figure 2F). Two alternative types of growth arrest, hyperosmotic shock (3M sorbitol) and sudden carbon starvation (culture washed during exponential growth and resuspended in carbon-free medium, then starved for 2 h, thus preventing adaptation during the stationary phase), also yielded similar protection from heat shocks (Figure 4A), suggesting that growth arrest by itself, independent of the underlying cause, is protective.

Oxidative damage contributes to heat-induced death

What are growth-arrested bacteria protected from? For eukaryotic microbes such as *S. cerevisiae* (Davidson and Schiestl, 2001; Davidson et al., 1996) and animals such as goldfish (Lushchak and Bagnyukova, 2006a, 2006b), it was shown that oxidative damage is involved in heat-induced stress and death. To reduce oxidative damage at high temperatures, *S. cerevisiae* exports antioxidants such as glutathione (Laman Trip and Youk, 2020). For bacteria, a similar connection between oxidative stress and temperature stress was hypothesized, based on the observation that temperature-sensitive mutants are hypersensitive to oxidative stress (Murata et al., 2011). To test whether oxidative stress is indeed involved in heat-induced death, we supplemented cultures in exponential growth at 37°C with glutathione and performed heat shocks. Strikingly, we found that glutathione-supplemented cultures in exponential growth survive 1,000-fold better than untreated controls (Figure 4B). This result indicates that growth inhibition alleviates lethal oxidative damage that would otherwise kill in heat shocks.

Oxidative damage is well known to induce aggregation (Lévy et al., 2019; Mirzaei and Regnier, 2008) and proteolysis (Davies and Lin, 1988; Pacifici and Davies, 1990), akin to the aggregation and degradation observed for MetA at high temperatures (Biran et al., 2000; Gur et al., 2002). We consequently wondered whether adding the antioxidant glutathione to our standard starvation and reinoculation protocol would influence lag times. We found a drastic reduction in lag times for cultures supplemented with glutathione, from 10.4 h to 1.4 h (Figure 4C). Because lag times are caused by degradation of MetA (Figure 2), this result suggests that oxidative damage is the trigger for MetA aggregation and consequent degradation. Similarly, glutathione prevents growth arrest at elevated temperatures in yeast (Laman Trip and Youk, 2020), suggesting that oxidative damage causes growth arrest more generally in microbes. To test whether growth arrest in yeast is also caused by methionine limitation or by a different mechanism, we tested whether growth arrest of *S. cerevisiae* at 39°C can be rescued with methionine. We found no difference in growth between methionine-supplemented cultures and controls (Figures S8A and S8B), showing that for yeast, growth arrest is caused by a different mechanism. The protective feature of growth arrest, however, is shared by yeast: While growing yeast (30°C) died by a factor of 500 during heat shocks, starving yeast largely survived (Figure S8C). Taken together, these findings show that employing growth inhibition to combat heat-induced death may be a more general strategy of microbes.

DISCUSSION

We have shown that breakdown of methionine biosynthesis at elevated temperatures causes growth arrest in *E. coli* in

environments without external methionine. Despite its fitness cost under habitable conditions, growth inhibition is beneficial for *E. coli* because it protects cells from heat-induced death when temperatures rise beyond 50°C. We demonstrated that this growth inhibition can be alleviated by simple point mutations and knockouts. We therefore suggest that it constitutes a self-controlled growth inhibition that has likely evolved as an active response to heat stress, orthogonal to the well-studied heat-shock response.

Relation to "viable but not culturable" and persistence states

Growth inhibition similar to the phenomenon described in our work is frequently encountered in a variety of microbes across the phylogenetic spectrum (Oliver, 2010) when exposed to stress conditions outside of optimal culture conditions (Xu et al., 1982; Oliver, 2005, 2010). A growing body of literature suggests the importance of growth inhibition in the context of "viable but not culturable" states (Oliver, 2005, 2010) and persistence (Balaban et al., 2004, 2019), particularly in food safety (Li et al., 2014b; Zhao et al., 2017) and antibiotic treatment (Balaban et al., 2004). However, pinning down mechanisms of how bacteria achieve growth inhibition and why such mechanisms have evolved has proved challenging (Pinto et al., 2015; Harms et al., 2016). Our results show that proteolytic regulation of basic biosynthetic pathways is an efficient strategy to robustly induce growth inhibition.

Shut-off of methionine synthesis is ideally suited to halt growth

While a lack of any amino acid would stop translation, lack of methionine specifically halts translation initiation because the majority of bacterial start codons code for *N*-formylmethionine (fMet), a direct derivative of methionine. Lack of other amino acids would halt elongation after initiation, leading to protein fragments that would need to be recycled by the cell. Furthermore, inhibition of translation triggers the stringent response alarmone (p)ppGpp (Potrykus and Cashel, 2008). This global regulator in bacteria inhibits synthesis of rRNA and tRNA (Lemke et al., 2011) transcription (Dalebroux and Swanson, 2012), as well as DNA replication (Schreiber et al., 1995; Wang et al., 2007), leading to a global shut-off in macromolecule synthesis. At the same time, the central metabolism and generation of energy-rich molecules are upstream of MetA so that cells are presumably well fueled to perform energy-dependent maintenance. This combination of inhibited biosynthesis but non-inhibited metabolism makes methionine an ideal bottleneck to induce growth inhibition in bacteria, which lack global regulators of growth, and we therefore speculate that this is the reason for the conservation of temperature-dependent methionine synthesis breakdown in bacteria across the phylogenetic spectrum (Ron, 1975; Wyman et al., 1975; Hwang et al., 2002; Rotem et al., 2013).

MetA is a biological "thermal fuse"

The temperature-induced degradation of MetA has a counterpart in electrical engineering: electrical devices are protected from excessive heat by "thermal fuses," which cut off electric current by physically disintegrating, typically by melting. The fuse has the role of an emergency protection, kicking in when other regulatory mechanisms have failed, in order to protect expensive components. In this analogy, first suggested by Price-Carter et al. (2005) for acid stress, we interpret MetA as a biological thermal fuse. If the benefit of increasing survival chances outweighs the cost of increased synthesis and missed potential for growth, the thermal fuse will have a net positive effect on fitness. The high expression levels combined with high degradation rates, as in the case of MetA, reflects a highly volatile strategy, typical for biological regulators (Gottesman and Maurizi, 1992). In fact, it is ideally suited to stressful conditions to ensure fast growth if conditions are bearable, while also quickly shutting off biosynthesis if conditions worsen.

Bet-hedging between growth and survival in anticipation of rare catastrophic events

The bistability in growth inhibition could play a vital role in optimizing fitness at elevated temperatures. Because both growth and growth arrest are stable, the bacterial population can split into two subpopulations, which manifests in our work as a lag time. If individual cells can switch between states of growth and arrest depending on the external environment and their internal methionine concentration, then according to the model the fitness of the population is optimized by partitioning the population into two subpopulations, a growing population and a growth-arrested population. Such a mixture of two distinct behaviors in a genetically homogeneous population of cells is a hallmark of bet-hedging strategies, typical for biological systems in unpredictable environments (Gardner et al., 2007; Veening et al., 2008; Verstraeten et al., 2015). Bet-hedging aims to increase long-term fitness beyond what would be possible for either pure strategies of growth or growth arrest. Thus, having a growth-inhibited subpopulation will allow microbes to survive sudden heat shocks while at the same time proliferating at subcritical temperatures, enabling them to robustly thrive at the edge of habitable conditions.

Limitations of the study

One of the key aspects that we were not able to resolve in this study is obtaining high-quality single-cell time-lapse data. Such data would have been useful to disentangle bulk lag times into contributions from single-cell lag times and non-growing populations, as well as allowing us to test whether individual bacteria enter a methionine-limited, growth-arrested state during exponential growth at elevated temperatures, as expected from the bistability of the model. We believe that the obstacle for growing bacteria in microfluidic chambers is that bacteria prime their medium, similar to yeast (Laman Trip and Youk, 2020). Diluting a culture at high temperatures into fresh medium dilutes the "primed medium" and arrests growth, even in batch culture (see Figure S3). Similarly, feeding fresh medium in microfluidics removes the "primed medium" and prevents cultures of *E. coli* from growing. For this reason we needed to settle for time-lapse microscopy using agar pads whereby culture with supernatant is plated to obtain a qualitative single-cell insight into the recovery dynamics.

STAR★METHODS

Detailed methods are provided in the online version of this paper and include the following:

- KEY RESOURCES TABLE
- RESOURCE AVAILABILITY
  - Lead contact
  - Materials availability
  - Data and code availability
- EXPERIMENTAL MODEL AND SUBJECT DETAILS
- METHOD DETAILS
  - Culture media
  - Growth protocol for E. coli
  - Growth protocol for S. cerevisiae
  - Protocol to induce lag times at high temperatures
  - Time-lapse microscopy
  - Live/dead stain
  - Heat shock protocol
  - Extended derivations
  - Separation of time-scales
- QUANTIFICATION AND STATISTICAL ANALYSIS
  - Quantification of lag time
  - Survival quantification
  - Statistical analysis

SUPPLEMENTAL INFORMATION

Supplemental information can be found online at https://doi.org/10.1016/j.celrep.2022.111290.

ACKNOWLEDGMENTS

This work was supported by the German Research Foundation (DFG) via the Excellence Cluster ORIGINS (through U.G.), and by the Life initiative of the Volkswagen Foundation (through U.G.). E.B. was supported by a DFG fellowship through the Graduate School of Quantitative Biosciences Munich. S.J.S. was supported by a Long-Term Fellowship (ALTF 782-2017) from the European Molecular Biology Organization and Long-Term Fellowship (LT000597/2018-L) from the Human Frontiers in Science Program. This project was supported by MIRA grant (5R35GM137895) to M.B.

AUTHOR CONTRIBUTIONS

S.J.S. and U.G. conceived this study. S.J.S., Z.G., E.B., and M.G.H. designed and performed experiments. Y.-F.C. constructed strains. S.J.S., M.B., and U.G. developed the theoretical model. S.J.S., Z.G., E.B., M.B., and U.G. wrote the paper. M.B. and U.G. funded and supervised the project.

DECLARATION OF INTERESTS

The authors declare no competing interests.

Received: September 7, 2021
Revised: January 10, 2022
Accepted: August 10, 2022
Published: August 30, 2022, corrected online January 15, 2025

SUPPORTING CITATIONS

The following references appear in the Supplemental Information: Hondorp and Matthews, 2006; Keseler et al., 2017; Madeira et al., 2019.

REFERENCES

Arsène, F., Tomoyasu, T., and Bukau, B. (2000). The heat shock response of Escherichia coli. Int. J. Food Microbiol. *55*, 3–9. https://doi.org/10.1016/S0168-1605(00)00206-3.

Baba, T., Ara, T., Hasegawa, M., Takai, Y., Okumura, Y., Baba, M., Datsenko, K.A., Tomita, M., Wanner, B.L., and Mori, H. (2006). Construction of *Escherichia coli* K-12 in-frame, single-gene knockout mutants: the Keio collection. Mol. Syst. Biol. *2*, 0008. https://doi.org/10.1038/msb4100050.

Balaban, N.Q., Merrin, J., Chait, R., Kowalik, L., and Leibler, S. (2004). Bacterial persistence as a phenotypic switch. Science *305*, 1622–1625. https://doi.org/10.1126/science.1099390.

Balaban, N.Q., Helaine, S., Lewis, K., Ackermann, M., Aldridge, B., Andersson, D.I., Brynildsen, M.P., Bumann, D., Camilli, A., Collins, J.J., et al. (2019). Definitions and guidelines for research on antibiotic persistence. Nat. Rev. Microbiol. *17*, 441–448. https://doi.org/10.1038/s41579-019-0196-3.

Bennett, B.D., Kimball, E.H., Gao, M., Osterhout, R., Van Dien, S.J., and Rabinowitz, J.D. (2009). Absolute metabolite concentrations and implied enzyme active site occupancy in Escherichia coli. Nat. Chem. Biol. *5*, 593–599. https://doi.org/10.1038/nchembio.186.

Biran, D., Brot, N., Weissbach, H., and Ron, E.Z. (1995). Heat shock-dependent transcriptional activation of the metA gene of Escherichia coli. J. Bacteriol. *177*, 1374–1379. https://doi.org/10.1128/JB.177.5.1374-1379.1995.

Biran, D., Gur, E., Gollan, L., and Ron, E.Z. (2000). Control of methionine biosynthesis in Escherichia coli by proteolysis. Mol. Microbiol. *37*, 1436–1443. https://doi.org/10.1046/j.1365-2958.2000.02097.x.

Bukau, B. (1993). Regulation of the Escherichia coli heat-shock response. Mol. Microbiol. *9*, 671–680. https://doi.org/10.1111/j.1365-2958.1993.tb01727.x.

Cherepanov, P.P., and Wackernagel, W. (1995). Gene disruption in Escherichia coli: TcR and KmR cassettes with the option of Flp-catalyzed excision of the antibiotic-resistance determinant. Gene *158*, 9–14. https://doi.org/10.1016/0378-1119(95)00193-A.

Csonka, L.N., Ikeda, T.P., Fletcher, S.A., and Kustu, S. (1994). The accumulation of glutamate is necessary for optimal growth of Salmonella typhimurium in media of high osmolality but not induction of the proU operon. J. Bacteriol. *176*, 6324–6333. https://doi.org/10.1128/jb.176.20.6324-6333.1994.

Dalebroux, Z.D., and Swanson, M.S. (2012). ppGpp: magic beyond RNA polymerase. Nat. Rev. Microbiol. *10*, 203–212. https://doi.org/10.1038/nrmicro2720.

Davidson, J.F., and Schiestl, R.H. (2001). Cytotoxic and genotoxic consequences of heat stress are dependent on the presence of oxygen in Saccharomyces cerevisiae. J. Bacteriol. *183*, 4580–4587. https://doi.org/10.1128/JB.183.15.4580-4587.2001.

Davidson, J.F., Whyte, B., Bissinger, P.H., and Schiestl, R.H. (1996). Oxidative stress is involved in heat-induced cell death in Saccharomyces cerevisiae. Proc. Natl. Acad. Sci. USA *93*, 5116–5121. https://doi.org/10.1073/pnas.93.10.5116.

Davies, K., and Lin, S.W. (1988). Degradation of oxidatively denatured proteins in Escherichia coli. Free Radic. Biol. Med. *5*, 215–223. https://doi.org/10.1016/0891-5849(88)90015-9.

Dill, K.A., Ghosh, K., and Schmit, J.D. (2011). Physical limits of cells and proteomes. Proc. Natl. Acad. Sci. USA *108*, 17876–17882. https://doi.org/10.1073/pnas.1114477108.

Friedman, N., Cai, L., and Xie, X.S. (2006). Linking stochastic dynamics to population distribution: an analytical framework of gene expression. Phys. Rev. Lett. *97*, 168302. https://doi.org/10.1103/PhysRevLett.97.168302.

Gardner, A., West, S.A., and Griffin, A.S. (2007). Is bacterial persistence a social trait? PLoS One *2*, e752. https://doi.org/10.1371/journal.pone.0000752.

Gottesman, S., and Maurizi, M.R. (1992). Regulation by proteolysis: energy-dependent proteases and their targets. Microbiol. Rev. *56*, 592–621.

Gur, E., Biran, D., Gazit, E., and Ron, E.Z. (2002). In vivo aggregation of a single enzyme limits growth of Escherichia coli at elevated temperatures. Mol. Microbiol. *46*, 1391–1397. https://doi.org/10.1046/j.1365-2958.2002.03257.x.

Harms, A., Maisonneuve, E., and Gerdes, K. (2016). Mechanisms of bacterial persistence during stress and antibiotic exposure. Science *354*, aaf4268. https://doi.org/10.1126/science.aaf4268.

Hondorp, E.R., and Matthews, R.G. (2006). Methionine. EcoSal Plus *2*. 7.

Hwang, B.-J., Yeom, H.-J., Kim, Y., and Lee, H.-S. (2002). Corynebacterium glutamicum utilizes both transsulfuration and direct sulfhydrylation pathways for methionine biosynthesis. J. Bacteriol. *184*, 1277–1286. https://doi.org/10.1128/JB.184.5.1277-1286.2002.

Jung, I.L., and Kim, I.G. (2003). Polyamines and glutamate decarboxylase-based acid resistance in *Escherichia coli*. J. Biol. Chem. *278*, 22846–22852. https://doi.org/10.1074/jbc.M212055200.

Keseler, I.M., Mackie, A., Santos-Zavaleta, A., Billington, R., Bonavides-Martínez, C., Caspi, R., Fulcher, C., Gama-Castro, S., Kothari, A., Krummenacker, M., et al. (2017). The EcoCyc database: reflecting new knowledge about Escherichia coli K-12. Nucleic Acids Res. *45*, D543–D550. https://doi.org/10.1093/nar/gkw1003.

Khan, A.U., Di Mascio, P., Medeiros, M.H., and Wilson, T. (1992). Spermine and spermidine protection of plasmid DNA against single-strand breaks induced by singlet oxygen. Proc. Natl. Acad. Sci. USA *89*, 11428–11430. https://doi.org/10.1073/pnas.89.23.11428.

Laman Trip, D.S., and Youk, H. (2020). Yeasts collectively extend the limits of habitable temperatures by secreting glutathione. Nat. Microbiol. *5*, 943–954. https://doi.org/10.1038/s41564-020-0704-2.

Laskowska, E., Kuczyńska-Wiśnik, D., Skórko-Glonek, J., and Taylor, A. (1996). Degradation by proteases Lon, Clp and HtrA, of Escherichia coli proteins aggregated in vivo by heat shock; HtrA protease action in vivo and in vitro. Mol. Microbiol. *22*, 555–571. https://doi.org/10.1046/j.1365-2958.1996.1231493.x.

Lemke, J.J., Sanchez-Vazquez, P., Burgos, H.L., Hedberg, G., Ross, W., and Gourse, R.L. (2011). Direct regulation of Escherichia coli ribosomal protein promoters by the transcription factors ppGpp and DksA. Proc. Natl. Acad. Sci. USA *108*, 5712–5717. https://doi.org/10.1073/pnas.1019383108.

Leuenberger, P., Ganscha, S., Kahraman, A., Cappelletti, V., Boersema, P.J., von Mering, C., Claassen, M., and Picotti, P. (2017). Cell-wide analysis of protein thermal unfolding reveals determinants of thermostability. Science *355*, eaai7825. https://doi.org/10.1126/science.aai7825.

Lévy, E., El Banna, N., Baïlle, D., Heneman-Masurel, A., Truchet, S., Rezaei, H., Huang, M.-E., Béringue, V., Martin, D., and Vernis, L. (2019). Causative links between protein aggregation and oxidative stress: a review. Int. J. Mol. Sci. *20*, 3896. https://doi.org/10.3390/ijms20163896.

Li, G.-W., Burkhardt, D., Gross, C., and Weissman, J.S. (2014a). Quantifying absolute protein synthesis rates reveals principles underlying allocation of cellular resources. Cell *157*, 624–635. https://doi.org/10.1016/j.cell.2014.02.033.

Li, L., Mendis, N., Trigui, H., Oliver, J.D., and Faucher, S.P. (2014b). The importance of the viable but non-culturable state in human bacterial pathogens. Front. Microbiol. *5*, 258. https://doi.org/10.3389/fmicb.2014.00258.

Lushchak, V.I., and Bagnyukova, T.V. (2006a). Temperature increase results in oxidative stress in goldfish tissues. 1. Indices of oxidative stress. Comp. Biochem. Physiol. C Toxicol. Pharmacol. *143*, 30–35. https://doi.org/10.1016/j.cbpc.2005.11.017.

Lushchak, V.I., and Bagnyukova, T.V. (2006b). Temperature increase results in oxidative stress in goldfish tissues. 2. Antioxidant and associated enzymes. Comp. Biochem. Physiol. C Toxicol. Pharmacol. *143*, 36–41. https://doi.org/10.1016/j.cbpc.2005.11.018.

Mackey, B.M., and Seymour, D.A. (1987). The effect of catalase on recovery of heat-injured DNA-repair mutants of Escherichia coli. J. Gen. Microbiol. *133*, 1601–1610. https://doi.org/10.1099/00221287-133-6-1601.

Madeira, F., Park, Y.M., Lee, J., Buso, N., Gur, T., Madhusoodanan, N., Basutkar, P., Tivey, A.R.N., Potter, S.C., Finn, R.D., and Lopez, R. (2019). The EMBL-EBI search and sequence analysis tools APIs in 2019. Nucleic Acids Res. *47*, W636–W641. https://doi.org/10.1093/nar/gkz268.

Marcén, M., Ruiz, V., Serrano, M.J., Condón, S., and Mañas, P. (2017). Oxidative stress in E. coli cells upon exposure to heat treatments. Int. J. Food Microbiol. *241*, 198–205. https://doi.org/10.1016/j.ijfoodmicro.2016.10.023.

Marcén, M., Cebrián, G., Ruiz-Artiga, V., Condón, S., and Mañas, P. (2019). Protective effect of glutathione on Escherichia coli cells upon lethal heat stress. Food Res. Int. *121*, 806–811. https://doi.org/10.1016/j.foodres.2018.12.063.

Maurizi, M.R. (1992). Proteases and protein degradation in Escherichia coli. Experientia *48*, 178–201. https://doi.org/10.1007/BF01923511.

Mirzaei, H., and Regnier, F. (2008). Protein:protein aggregation induced by protein oxidation. J. Chromatogr. B Anal. Technol. Biomed. Life Sci. *873*, 8–14. https://doi.org/10.1016/j.jchromb.2008.04.025.

Mordukhova, E.A., and Pan, J.-G. (2014). Stabilization of homoserine-O-succinyltransferase (MetA) decreases the frequency of persisters in Escherichia coli under stressful conditions. PLoS One *9*, e110504. https://doi.org/10.1371/journal.pone.0110504.

Mordukhova, E.A., Lee, H.-S., and Pan, J.-G. (2008). Improved thermostability and acetic acid tolerance of Escherichia coli via directed evolution of homoserine o-succinyltransferase. Appl. Environ. Microbiol. *74*, 7660–7668. https://doi.org/10.1128/AEM.00654-08.

Mordukhova, E.A., Kim, D., and Pan, J.-G. (2013). Stabilized homoserine o-succinyltransferases (MetA) or L-methionine partially recovers the growth defect in Escherichia coli lacking ATP-dependent proteases or the DnaK chaperone. BMC Microbiol. *13*, 179. https://doi.org/10.1186/1471-2180-13-179.

Murata, M., Fujimoto, H., Nishimura, K., Charoensuk, K., Nagamitsu, H., Raina, S., Kosaka, T., Oshima, T., Ogasawara, N., and Yamada, M. (2011). Molecular strategy for survival at a critical high temperature in Eschierichia coli. PLoS One *6*, e20063. https://doi.org/10.1371/journal.pone.0020063.

Neidhardt, F.C. (1996). Escherichia coli and Salmonella: Cellular and Molecular Biology (ASM Press).

Nierhaus, D., and Nierhaus, K.H. (1973). Identification of the chloramphenicol-binding protein in Escherichia coli ribosomes by partial reconstitution. Proc. Natl. Acad. Sci. USA *70*, 2224–2228. https://doi.org/10.1073/pnas.70.8.2224.

Nonaka, G., Blankschien, M., Herman, C., Gross, C.A., and Rhodius, V.A. (2006). Regulon and promoter analysis of the E. coli heat-shock factor, σ32, reveals a multifaceted cellular response to heat stress. Genes Dev. *20*, 1776–1789. https://doi.org/10.1101/gad.1428206.

Oliver, J.D. (2005). The viable but nonculturable state in bacteria. J. Microbiol. *43*, 93–100.

Oliver, J.D. (2010). Recent findings on the viable but nonculturable state in pathogenic bacteria. FEMS Microbiol. Rev. *34*, 415–425. https://doi.org/10.1111/j.1574-6976.2009.00200.x.

Pacifici, R.E., and Davies, K.J.A. (1990). Protein degradation as an index of oxidative stress. In Methods in Enzymology (Academic Press), pp. 485–502.

Pinto, D., Santos, M.A., and Chambel, L. (2015). Thirty years of viable but nonculturable state research: unsolved molecular mechanisms. Crit. Rev. Microbiol. *41*, 61–76. https://doi.org/10.3109/1040841X.2013.794127.

Potrykus, K., and Cashel, M. (2008). Still magical? Annu. Rev. Microbiol. *62*, 35–51. https://doi.org/10.1146/annurev.micro.62.081307.162903.

Price-Carter, M., Fazzio, T.G., Vallbona, E.I., and Roth, J.R. (2005). Polyphosphate kinase protects Salmonella enterica from weak organic acid stress. J. Bacteriol. *187*, 3088–3099. https://doi.org/10.1128/JB.187.9.3088-3099.2005.

Privalle, C.T., and Fridovich, I. (1987). Induction of superoxide dismutase in Escherichia coli by heat shock. Proc. Natl. Acad. Sci. USA *84*, 2723–2726. https://doi.org/10.1073/pnas.84.9.2723.

Richter, K., Haslbeck, M., and Buchner, J. (2010). The heat shock response: Life on the verge of death. Mol. Cell *40*, 253–266. https://doi.org/10.1016/j.molcel.2010.10.006.

Ron, E.Z. (1975). Growth rate of Enterobacteriaceae at elevated temperatures: limitation by methionine. J. Bacteriol. *124*, 243–246. https://doi.org/10.1128/JB.124.1.243-246.1975.

Ron, E.Z., and Davis, B.D. (1971a). Growth rate of Escherichia coli at elevated temperatures: limitation by methionine. J. Bacteriol. *107*, 391–396.

Ron, E.Z., and Shani, M. (1971). Growth rate of Escherichia coli at elevated temperatures: reversible inhibition of homoserine trans-succinylase. J. Bacteriol. *107*, 397–400.

Rotem, O., Biran, D., and Ron, E.Z. (2013). Methionine biosynthesis in Agrobacterium tumefaciens: study of the first enzyme. Res. Microbiol. *164*, 12–16. https://doi.org/10.1016/j.resmic.2012.10.005.

Schreiber, G., Ron, E.Z., and Glaser, G. (1995). ppGpp-mediated regulation of DNA replication and cell division in Escherichia coli. Curr. Microbiol. *30*, 27–32. https://doi.org/10.1007/BF00294520.

Shah, P., and Swiatlo, E. (2008). A multifaceted role for polyamines in bacterial pathogens. Mol. Microbiol. *68*, 4–16. https://doi.org/10.1111/j.1365-2958.2008.06126.x.

Soupene, E., van Heeswijk, W.C., Plumbridge, J., Stewart, V., Bertenthal, D., Lee, H., Prasad, G., Paliy, O., Charernnoppakul, P., and Kustu, S. (2003). Physiological studies of Escherichia coli strain MG1655: growth defects and apparent cross-regulation of gene expression. J. Bacteriol. *185*, 5611–5626. https://doi.org/10.1128/JB.185.18.5611-5626.2003.

Strogatz, S.H. (2018). Nonlinear Dynamics and Chaos with Student Solutions Manual: With Applications to Physics, Biology, Chemistry, and Engineering (CRC press).

Taniguchi, Y., Choi, P.J., Li, G.-W., Chen, H., Babu, M., Hearn, J., Emili, A., and Xie, X.S. (2010). Quantifying E. coli proteome and transcriptome with single-molecule sensitivity in single cells. Science *329*, 533–538. https://doi.org/10.1126/science.1188308.

Veening, J.-W., Smits, W.K., and Kuipers, O.P. (2008). Bistability, epigenetics, and bet-hedging in bacteria. Annu. Rev. Microbiol. *62*, 193–210. https://doi.org/10.1146/annurev.micro.62.081307.163002.

Verstraeten, N., Knapen, W.J., Kint, C.I., Liebens, V., Van den Bergh, B., Dewachter, L., Michiels, J.E., Fu, Q., David, C.C., Fierro, A.C., et al. (2015). Obg and membrane depolarization are part of a microbial bet-hedging strategy that leads to antibiotic tolerance. Mol. Cell *59*, 9–21. https://doi.org/10.1016/j.molcel.2015.05.011.

Wang, J.D., Sanders, G.M., and Grossman, A.D. (2007). Nutritional control of elongation of DNA replication by (p)ppGpp. Cell *128*, 865–875. https://doi.org/10.1016/j.cell.2006.12.043.

Wyman, A., Shelton, E., and Paulus, H. (1975). Regulation of homoserine transacetylase in whole cells of Bacillus polymyxa. J. Biol. Chem. *250*, 3904–3908.

Xu, H.-S., Roberts, N., Singleton, F.L., Attwell, R.W., Grimes, D.J., and Colwell, R.R. (1982). Survival and viability of nonculturable Escherichia coli and Vibrio cholerae in the estuarine and marine environment. Microb. Ecol. *8*, 313–323. https://doi.org/10.1007/BF02010671.

Yura, T., and Nakahigashi, K. (1999). Regulation of the heat-shock response. Curr. Opin. Microbiol. *2*, 153–158. https://doi.org/10.1016/S1369-5274(99)80027-7.

Zhao, X., Zhong, J., Wei, C., Lin, C.-W., and Ding, T. (2017). Current perspectives on viable but non-culturable state in foodborne pathogens. Front. Microbiol. *8*, 580. https://doi.org/10.3389/fmicb.2017.00580.

STAR★METHODS

KEY RESOURCES TABLE

REAGENT or RESOURCE	SOURCE	IDENTIFIER
Bacterial and virus strains		
E. coli K-12, WT	Soupene et al. (2003)	NCM3722
E. coli K-12, $MetA_{I229Y}$	This paper	YCE55
E. coli K-12, $MetA_{LYD}$ (I124L-I229Y-N267D)	This paper	YCE57
E. coli K-12, Δhslv, ΔclpP, Δlon:Kan	This paper	YCE134
Chemicals, peptides, and recombinant proteins		
K_2SO_4	Carl Roth, Karlsruhe, Germany	Cat#P022.2
$K_2HPO_4 \cdot 3H_2O$	Carl Roth, Karlsruhe, Germany	Cat#6878.1
KH_2PO_4	Carl Roth, Karlsruhe, Germany	Cat#3904.3
$MgSO_4 \cdot 7H_2O$	Carl Roth, Karlsruhe, Germany	Cat#P027.1
NaCl	Carl Roth, Karlsruhe, Germany	Cat#3957.1
NH_4Cl	Carl Roth, Karlsruhe, Germany	Cat#K298.2
L-Methionine	Carl Roth, Karlsruhe, Germany	Cat#1702.1
L-Glutathione Reduced	Carl Roth, Karlsruhe, Germany	Cat#6832.1
Chloramphenicol	Carl Roth, Karlsruhe, Germany	Cat#3886.3
Sorbitol	Sigma-Aldrich, St. Louis, MO, USA	Cat#S1876-500G
Critical commercial assays		
BacLight!LIVE/DEAD	Thermo Fisher Scientific Inc., Waltham, Massachusetts, USA	Cat#L34856
Deposited data		
Experimental data for all figures	This paper	https://doi.org/10.57760/sciencedb.02073
Experimental models: Organisms/strains		
S. cerevisiae	Michael Springer Lab, Harvard Medical School	S288C
Software and algorithms		
MATLAB scripts to generate Figures 3B, S7A, and S7B	This paper.	https://doi.org/10.57760/sciencedb.02073

RESOURCE AVAILABILITY

Lead contact

Further information and requests for resources and reagents should be directed to the lead contact, Ulrich Gerland (gerland@tum.de).

Materials availability

Strains YCE55, YCE57 and YCE134 are available upon request, subject to a material transfer agreement (MTA), from Markus Basan (markus@hms.harvard.edu).

Data and code availability

- Experimental data for all figures have been deposited to ScienceDB and is publicly available as of the date of publication. The DOI is listed in the key resources table.
- All original code has been deposited to ScienceDB and is publicly available as of the date of publication. The DOI is listed in the key resources table.
- Any additional information required to reanalyze the data reported in this paper is available from the lead contact upon request.

EXPERIMENTAL MODEL AND SUBJECT DETAILS

All bacterial strains used in this study are derived from wild type *E. coli* K-12 strain NCM3722 (Soupene et al., 2003). Amino acid substitutions $MetA_{I229Y}$ and $MetA_{LYD}$ (containing point mutations I124L-I229Y-N267D) in strains I229Y and LYD (Mordukhova et al., 2013)

were transferred to NCM3722 ΔMetA via P1 transduction to yield strains YCE55 (NCM3722 $metA_{I229Y}$) and YCE57 (NCM3722 $metA_{LYD}$), using methionine as a selective marker. YCE134 was created by consecutivelty transferring knock-out mutations from the Keio collection (Baba et al., 2006) of *hslV*, *clpP* and *lon* to NCM3722 via P1 transduction, whereas each transformation was followed by removal of the kanamycin restistenence cassette via FLP recombination with PCP20 (Cherepanov and Wackernagel, 1995), yielding the final strain YCE134 (NCM3722, Δhslv, ΔclpP, Δlon:Kan). The yeast strain used in this study is *Saccharomyces cereviseae* S288C.

METHOD DETAILS

Culture media

The culture medium for *E. coli* used in this study is based on N^-C^- minimal medium (Csonka et al., 1994), containing K_2SO_4 (1 g), $K_2HPO_4 \cdot 3H_2O$ (17.7 g), KH_2PO_4 (4.7 g), $MgSO_4 \cdot 7H_2O$ (0.1 g) and NaCl (2.5 g) per liter. The medium was supplemented with 20 mM NH_4Cl, as nitrogen source, and 5 to 10 mM glycerol, as the sole carbon source. *S. cerevisiae* were cultured in yeast nitrogen base medium (without amino acids) and supplemented with 0.5% glucose. All chemicals were purchased from Carl Roth, Karlsruhe, Germany. When needed, 0.1 mg/mL ampicillin (stock prepared fresh and stored at −20°C) and/or 0.067 mM methionine (stock stored at 4°C) were added to the culture.

Growth protocol for E. coli

Cells were taken from a −80°C glycerol stock, streaked out on an LB agar plate and incubated around 12 h at 37°C. A single colony was picked and grown in batch culture. For temperatures up to 39°C, cells were grown first on LB at the desired temperature (seed culture). Before reaching starvation, they were diluted and inoculated into pre-warmed minimal medium supplemented with glycerol (pre-culture). Cells grew in the pre-culture for several doublings to ensure exponential growth and were then diluted and inoculated into pre-warmed glycerol minimal medium (experimental culture). Inoculation into the latter was chosen such that cells perform at least three additional doublings in the experimental culture before growth was measured. For high temperatures (above 39°C), the seed culture medium used was glycerol minimal medium with 1% LB in order to help the cells transition into the pre-culture.

For small culture volumes, 5 mL of culture were grown in 20 mm × 150 mm glass test tubes (Fisher Scientific, Hampton, NH, USA) with disposable, polypropylene Kim-Kap closures (Kimble Chase, Vineland, NJ, USA). Larger volumes, 25 mL, 50 mL and 100 mL were grown in 125 mL, 250 mL and 500 mL baffled Erlenmeyer flasks (Carl Roth, Karlsruhe, Germany), respectively, and Kim-Kap closures. All cultures were grown in a shaking water bath (WSB-30, Witeg, Wertheim, Germany) with water bath preservative (Akasolv, Akadia, Mannheim, Germany).

Growth protocol for S. cerevisiae

Cells were streaked from a −80°C glycerol stock onto a YPD agar plate and incubated for approximately 30 h at 30°C. A single colony was picked and grown in batch culture with 4 mL NBM containing 1% YPD. Where necessary, the culture was supplemented with methionine (0.067 mM). All cultures were incubated in a shaking water bath with the culture tubes angled parallel to the direction of shaking. The culture tubes and shaking water bath used were identical to those used for the cultivation of *E. coli*.

Protocol to induce lag times at high temperatures

Bacteria were first grown in minimal medium supplemented with glycerol as a carbon substrate, as described above, at the desired temperature (37–45°C). After carbon depletion, cultures starved for 1 h–24 h. Then, cultures were diluted into fresh N^-C^- supplemented with glycerol and NH_4Cl and allowed to recover.

Time-lapse microscopy

Microscopy was performed using agar pads in glass-bottom dishes. Agar pads contained medium identical to the culture medium, N^-C^- supplemented with 20 mM NH_4Cl, 20 mM Glycerol and 2% low melting point agarose (Carl Roth, Karlsruhe, Germany). Cells were diluted and pipetted on the prewarmed agar pad and kept in the incubator. After the surface of the agar pad had dried, the agar pad was flipped on the glass window of a prewarmed glass bottom dish. The glass bottom dishes were sealed with parafilm to reduce evaporation.

Time-lapse microscopy was performed using a Nikon Ti-E microscope controlled by NIS-Elements (Nikon, Tokyo, Japan). We used a phase contrast Plan Apo 100× oil objective, with numerical aperture of 1.45 and a refractive index of 1.515 (Nikon, Tokyo, Japan) and a SCMOS camera (Zyla-5.5, Andor, Belfast, Northern Ireland) with a binning of 1 × 1, a readout rate of 200 MHz and an exposure time of 200 ms. Conversion gain was set on 1/3 Dual gain and the spurious noise filter was activated. The calibration from length units to pixels was defined as 0.07 μm/px. Measurements were performed with activated perfect focus system and a PriorScan III drive stage. Temperature control was set by the Okolab Cage Incubation System and confirmed with manual temperature measurements. Cell growth was monitored for 24 h with continuous acquisition of phase-contrast and fluorescence images every 30 min at the desired temperature, e.g. 45°C. Note that the fractions of recovering and non-recovering bacteria measured by recovery on agar pads are likely influenced by a change in bacterial density and supernatant, similar to Figure S3.

Live/dead stain

Commercial BacLight®LIVE/DEAD (Thermo Fisher Scientific Inc., Waltham, Massachusetts, USA) staining was used when cells were microscopically imaged, according to manufacturing specifications.

Heat shock protocol

Heat shocks were performed by transferring batch cultures (5 mL culture volume in a 20 mm × 150 mm borosilicate glass tube (Fisher Scientific, NH, USA)) from one water bath to another (WSB-30, Witeg, Wertheim, Germany). Water baths were pre-set and equilibrated at the desired temperatures.

Numerical analysis of the model

The numerical solution in Figure 3B was obtained by numerically integrating Equations (1–3) using the nonstiff differential equation solver *ode45* in Matlab (Mathworks, Natick, MA, USA). Initial conditions were $c_{\mathrm{met}}(0) = 0$ and $\varphi_{\mathrm{MetA}}(0)$ ranging from $2{\cdot}10^{-5}$ to $2{\cdot}10^{-4}$. The parameters used in the calculations were $a_1 = 4.06\,\mathrm{M}^{-1}$, $a_2 = 3.1{\cdot}10^{-5}$, $a_3 = 148\,\mathrm{M}^{-2}$, $\chi_{\mathrm{MetA}} = 2.79{\cdot}10^{-3}$, $K_{\mathrm{M}} = 10^{-6}$ M, see Table S2.

The phase diagrams in Figure S7 were calculated by solving Equation (16) using the *solve* function in Matlab (Mathworks, Natick, MA, USA). We shaded the regions according to the number of stable fixed-points at concentrations higher or equal to zero. One solution at $c^{*}_{\mathrm{met}} = 0$ (stable) was denoted 'non-growing region'. Two zeros, $c^{*,1}_{\mathrm{met}} = 0$ (unstable) and $c^{*,2}_{\mathrm{met}} > 0$ (stable) was denoted 'growth region'. Three zeros was denoted as the 'bistable region'. If methionine influx was included, Figure S7B, one stable solution at $c^{*}_{\mathrm{met}} > 0$ means that cells can grow on external methionine. This region was shaded 'grey to white' to symbolize the growth rate dependence on the methionine influx. The parameters used in the calculations were $a_1 = 4.06\,\mathrm{M}^{-1}$, $a_2 = 3.1{\cdot}10^{-5}$, $a_3 = 148\,\mathrm{M}^{-2}$, $\chi_{\mathrm{MetA}} = 2.79{\cdot}10^{-3}$, $K_{\mathrm{M}} = 10^{-6}$ M, see Table S2.

Extended derivations

In this section of the methods, we will derive theoretical solutions for the model. In particular, we focus here on the stability analysis, the MetA recovery threshold and the derivation of the lag times. In addition, we make a detailed estimation of the theoretical parameters from measurements in the literature.

Stability analysis

Here we discuss the stability of the non-linear equation system proposed in Equations (1–3). The standard approach to stability analysis requires derivation of the two nullclines of the system, where 1) the methionine concentration and 2) the active relative MetA abundance are constant (Strogatz, 2018). At the intersection of the two nullclines, we find the 'fixed points'. When the system is evolving, the cells will relax towards the stable fixed points (and away from the unstable fixed points). In our case, the possible stable fixed-point positions are growth or growth arrest and their existence will be discussed thereafter. We will first derive the nullclines and then the criteria for the existence of the fixed points.

Derivation of the nullclines

In Equation (2) we derived the dynamics of the internal methionine concentration as

$$\frac{\mathrm{d}c_{\mathrm{met}}}{\mathrm{d}t} = j_{\mathrm{MetA}}(\varphi_{\mathrm{MetA}}) + j_{\mathrm{in}} - j_{\mathrm{p}}(c_{\mathrm{met}}) - j_{\mathrm{d}}(c_{\mathrm{met}}) - \mu c_{\mathrm{met}}, \qquad \text{(Equation 5)}$$

With the individual contributions being

$$j_{\mathrm{MetA}} = h\varphi_{\mathrm{MetA}} \qquad \text{(Equation 6)}$$

$$j_{\mathrm{p}} = c^{\mathrm{pro}}_{\mathrm{met}} k_{\mathrm{p}} c_{\mathrm{met}} = c^{\mathrm{pro}}_{\mathrm{met}} \mu \qquad \text{(Equation 7)}$$

$$j_{\mathrm{d}} = k_{\mathrm{d}} u(c_{\mathrm{met}}) \qquad \text{(Equation 8)}$$

$$j_{\mathrm{in}} = \mathrm{const} > 0 \qquad \text{(Equation 9)}$$

and

$$\mu = k_{\mathrm{p}} c_{\mathrm{met}}, \qquad \text{(Equation 10)}$$

$$u(c_{\mathrm{met}}) = c_{\mathrm{met}}/(K_{\mathrm{M}} + c_{\mathrm{met}}). \qquad \text{(Equation 11)}$$

The production flux $j_{MetA} = h\varphi_{MetA}$ equals the production rate h times the relative MetA abundance φ_{MetA}, because MetA is the limiting step in synthesis (Ron and Davis, 1971a). Here, relative MetA abundance φ_{MetA} is defined as the fraction of the proteome that is MetA. Uptake flux j_{in} depends on the presence of methionine and metabolites containing methionine in the medium. The methionine flux to protein synthesis $j_p = c_{met}^{pro}\,\mu$ is calculated by assuming that cells maintain a constant protein density, in which case the flux needs to be sufficient to prevent dilution of the 'methionine concentration bound in proteins' c_{met}^{pro}, if the cell is growing at rate μ. We estimate an internal methionine concentration of $c_{met}^{pro} = 27.5$ mM from the codon frequency of methionine (3.2%) and a typical protein concentration of about 0.125 g/ml , see Table S2. Finally, we assume that growth rate is proportional to the methionine concentration, $\mu = k_p c_{met}$, in Equation (10). This approximation is valid in the regime where methionine concentration is low. We chose this approximation because the model is designed to describe the bistability in growth, where the recovery from low MetA abundancies and low methionine concentrations is crucial. This approximation breaks down during regular growth, which could be resolved with a saturating term in Equation (10).

Finally, we consider that methionine is consumed for S-adenosyl-methionine (SAM) synthesis, the major methyl donor of the cell. See Figure S6 for a summary of the methionine pathway. While much of this SAM is recycled back to methionine, a part of it is used for biosynthesis of polyamines, such as spermine and spermidine, which are important for survival in stress conditions (Khan et al., 1992; Jung and Kim, 2003; Shah and Swiatlo, 2008). Of these metabolites, spermidine is present at a particularly high intracellular concentration, $c_{spe} = 1.4$ mM (Neidhardt, 1996). Because one methionine is consumed per spermidine, we can estimate the fraction of the methionine flux that is used for spermidine synthesis as $c_{spe}/c_{met}^{pro} = 1.4\,\text{mM}/27.5\,\text{mM} = 5\%$. Since polyamine synthesis is an overall small part of the cell's biomass, we assume that the 'drainage flux', j_d, saturates at some level and model it as a saturating function of the internal methionine concentration, $j_d = k_d\, c_{met}/(c_{met} + K_M)$, with k_d being the maximum efflux rate and K_M the Michaelis constant. Efflux of methionine from the cell, either by passive diffusive loss or by active export, could also contribute to the drain of internal methionine, but will be neglected here. If existent, they would effectively increase the drainage flux j_d. The combination of all metabolite fluxes determines the dynamics of the methionine concentration, the limiting bottleneck at elevated temperatures.

The nullcline of the methionine concentration is defined as the manifold in the space of φ_{MetA} and c_{met}, in which $dc_{met}/dt = 0$. Setting Equation (5) to zero, we get

$$\frac{dc_{met}}{dt} = f_1(\varphi_{MetA}, c_{met}) = h\varphi_{MetA} + j_{in} - c_{met}^{pro} k_p c_{met} - k_d u(c_{met}) - k_p c_{met}^2 = 0. \quad \text{(Equation 12)}$$

By solving this equation for φ_{MetA} and defining new parameters $a_1 = c_{met}^{pro} k_p h^{-1}$, $a_2 = k_d h^{-1}$ and $a_3 = k_p h^{-1}$, as well as $\tilde{j}_{in} = j_{in} h^{-1}$, we derive the nullcline of the methionine concentration,

$$g_{met}(c_{met}) = \varphi_{MetA} = a_1 c_{met} + a_2 u(c_{met}) + a_3 c_{met}^2 - \tilde{j}_{in}. \quad \text{(Equation 13)}$$

The second component of the model is the dynamics of the relative MetA abundance, φ_{MetA}. MetA is synthesized during growth at rate $\chi_{MetA}\mu$, where χ_{MetA} is the fraction of the newly synthesized proteome that is MetA. Since we are interested in the regime of low methionine abundance, we assume that χ_{MetA} is set to a constant, maximum value, i.e., full expression. In addition to dilution by growth, $\mu\varphi_{MetA}$, the relative MetA abundance decays, at a rate that we assume to be identical for all cells at the same temperature, $\eta(T)\varphi_{MetA}$ (Biran et al., 2000; Mordukhova et al., 2013). The decay rate $\eta(T)$ is temperature T dependent (Mordukhova et al., 2013), ATP dependent (Biran et al., 2000) and includes any process that renders MetA unfunctional, from degradation (Biran et al., 2000) to thermal aggregation (Gur et al., 2002). Combined, the dynamics of the relative MetA abundance gives Equation (3), which we set to zero to obtain the nullcline

$$\frac{d\varphi_{MetA}}{dt} = f_2(\varphi_{MetA}, c_{met}) = \chi_{MetA}\mu(c_{met}) - (\eta(T) + \mu(c_{met}))\varphi_{MetA} = 0. \quad \text{(Equation 14)}$$

By solving for φ_{MetA}, we obtain the nullcine for the active relative MetA abundance to be

$$g_{MetA}(c_{met}) = \varphi_{MetA} = \chi_{MetA}\frac{c_{met}}{\tilde{\eta} + c_{met}}, \quad \text{(Equation 15)}$$

where we define a new variable $\tilde{\eta} = \eta k_p^{-1}$ and use $\mu = k_p c_{met}$ from Equation (1).

Stability criteria

The fixed points of the system are found at the intersection of both nullclines $g_{met}(c_{met}) = g_{MetA}(c_{met})$, i.e.

$$\chi_{MetA}\frac{c_{met}^*}{\tilde{\eta} + c_{met}^*} = \varphi_{MetA} = a_1 c_{met}^* + a_2 u(c_{met}^*) + a_3 c_{met}^{*2} - \tilde{j}_{in}, \quad \text{(Equation 16)}$$

where c_{met}^* is the fixed-point of the internal methionine concentration. The fixed-point of the relative MetA abundance φ_{MetA}^* can then be obtained by plugging in c_{met}^* into either nullcline. If we then solve the fixed-points of Equation (16) numerically, we can get an exact

solution for the growth fixed point. This numerical solution is shown in Figure S7.

Depending on the parameter regime, there are either one, two or three fixed-points in the regime $c_{met} \geq 0$ and $\varphi_{MetA} \geq 0$. We can get vital information about the system by calculating stability criteria analytically. We consider the simplest case of no external methionine influx $\tilde{j}_{in} = 0$, where the trivial solution of the fixed-point equation, Equation (16), is $c^d_{met} = 0$ and $\varphi^d_{MetA} = 0$. This fixed-point corresponds to dormancy, thus the superscript 'd', because in this case the steady state growth rate is zero, $\mu^d = k_p c^d_{met} = 0$. This fixed-point can either be stable, i.e. the cell will stop growing when close to this fixed-point, or unstable, i.e. the cell will start growing, even at very low c_{met} and φ_{MetA} levels. The stability can be checked using the Jacobian matrix of the system, defined as

$$J = \begin{pmatrix} \frac{\partial f_1}{\partial c_{met}} & \frac{\partial f_1}{\partial \varphi_{MetA}} \\ \frac{\partial f_2}{\partial c_{met}} & \frac{\partial f_2}{\partial \varphi_{MetA}} \end{pmatrix} \quad \text{(Equation 17)}$$

At the trivial fixed point $c^d_{met} = 0$ and $\varphi^d_{MetA} = 0$, we find

$$J = \begin{pmatrix} -h(a_1 + a_2/K_M) & h \\ \chi_{MetA} k_p & -\eta \end{pmatrix}. \quad \text{(Equation 18)}$$

The stability of the fixed point can then be checked by computing the trace

$$\tau = \frac{\partial f_1}{\partial c_{met}} + \frac{\partial f_2}{\partial \varphi_{MetA}} \quad \text{(Equation 19)}$$

and determinant

$$\Delta = \frac{\partial f_1}{\partial c_{met}} \frac{\partial f_2}{\partial \varphi_{MetA}} - \frac{\partial f_1}{\partial \varphi_{MetA}} \frac{\partial f_2}{\partial c_{met}} \quad \text{(Equation 20)}$$

of the Jacobian matrix (Strogatz, 2018). Because the trace $\tau = -(h(a_1 + a_2/K_M) + \eta)$ is negative, the stability is determined solely by the sign of the determinant $\Delta = h(a_1 + a_2/K_M)\eta - h\chi_{MetA}k_p$. If $\Delta > 0$, then the dormancy fixed-point is stable. This condition is met if

$$\eta > \frac{\chi_{MetA} k_p}{(a_1 + a_2/K_M)}, \quad \text{(Equation 21)}$$

which can be formulated in terms of the original parameters as

$$\eta > \frac{\chi_{MetA} h}{c^{pro}_{met} + k_d/(k_p K_M)}. \quad \text{(Eqaution 22)}$$

To get an analytical estimate for the stability criterium of the growth fixed-point, we make several simplifying assumptions. We first note that the relative MetA abundance nullcline $g_{MetA}(c_{met})$ levels to a constant, $g_{MetA}(c_{met} \to \infty) \to \chi_{MetA} = \text{const}$, for high methionine concentrations, see Equation (14), while the methionine nullcline $g_{met}(c_{met})$ increases monotonically to infinity in the same limit, $g_{met}(c_{met} \to \infty) \to \infty$, see Equation (12). Thus, if at low methionine concentrations, the methionine nullcline $g_{met}(c_{met})$ is lower than the relative MetA abundance nullcline $g_{MetA}(c_{met})$, these two nullclines will cross and create a fixed-point at finite growth, $c^g_{met} > 0$ and $\varphi^g_{MetA} > 0$, where the superscript 'g' stands for growth.

There are two possibilities that the methionine nullcline $g_{met}(c_{met})$ can be lower than the relative MetA abundance nullcline $g_{MetA}(c_{met})$. The first option is that for very low methionine concentration, $0 < c_{met} \ll K_M$, the methionine nullcline increases less than the relative MetA abundance nullcline, $dg_{met}/dc_{met} < dg_{MetA}/dc_{met}$. Testing this was the essence of the stability analysis done for the non-growing fixed-point in this section: if the dormancy fixed point is stable, $dg_{met}/dc_{met} > dg_{MetA}/dc_{met}$; if the dormancy fixed point is unstable, $dg_{met}/dc_{met} < dg_{MetA}/dc_{met}$. The second option is that, at a higher methionine concentration, the methionine nullcline $g_{met}(c_{met})$ is again lower than the MetA nullcline $g_{MetA}(c_{met})$. We estimate the regime where this happens, by comparing the two nullclines at relatively low methionine concentrations $K_M \ll c_{met} \ll c^g_{met}$, in the regime where the drain has already saturated, i.e., $u(K_M \ll c_{met}) = 1$, but the methionine concentration is still low compared to the steady state, c^g_{met}.

In this regime, the methionine nullcline can be approximated as $g_{met}(c_{met}) \approx a_1 c_{met} + a_2$, by omitting quadratic terms in Equation (12). The relative MetA abundance nullcline in the same regime can be approximated as, $g_{MetA}(c_{met}) \approx \chi_{MetA}\tilde{\eta}^{-1} c_{met}$, when we omit higher order terms in Equation (14). Combined, these two approximations yield that, if $a_1 c_{met} + a_2 < \chi_{MetA}\tilde{\eta}^{-1} c_{met}$, then the methionine nullcline lies below the MetA nullcline.

If we take $a_2 \approx 0$, then we can estimate an upper limit,

$$\tilde{\eta} < \frac{\chi_{MetA}}{a_1} \quad \text{(Equation 23)}$$

or in the original parameters,

$$\eta < \frac{\chi_{\mathrm{MetA}} h}{c_{\mathrm{met}}^{\mathrm{pro}}}, \quad \text{(Equation 24)}$$

for the degradation rate in this regime.

From the above analysis we conclude that three distinct regimes exist. First, if

$$\eta < \frac{\chi_{\mathrm{MetA}} h}{c_{\mathrm{met}}^{\mathrm{pro}} + k_{\mathrm{d}}/(k_{\mathrm{p}} K_{\mathrm{M}})}, \quad \text{(Eqaution 25)}$$

then only the growing state is stable, and all cells in the population will grow. Second, if

$$\frac{\chi_{\mathrm{MetA}} h}{c_{\mathrm{met}}^{\mathrm{pro}} + k_{\mathrm{d}}/(k_{\mathrm{p}} K_{\mathrm{M}})} < \eta < \frac{\chi_{\mathrm{MetA}} h}{c_{\mathrm{met}}^{\mathrm{pro}}} \quad \text{(Equation 26)}$$

then both a stable growth and dormancy fixed-points exists, and the culture can split into two subpopulations. Third, if

$$\eta > \frac{\chi_{\mathrm{MetA}} h}{c_{\mathrm{met}}^{\mathrm{pro}}} \quad \text{(Equation 27)}$$

then only the dormant state is stable and the entire population will converge to growth arrest.

Calculation of the recovery threshold

In the case that the environment permits two stable fixed-points, growth and dormancy, the question is: in which state will an individual cell end? To address this question, we will calculate the necessary relative MetA abundance for recovery, called the "recovery threshold". Above this threshold, the cell will have enough MetA to start producing more methionine and, conversely, more MetA. Below the threshold, too much methionine is drained, the degradation of MetA is faster than the production of new MetA and the cells will end in a stable state of dormancy.

Separation of time-scales

In starvation, according to the model, the internal metabolite concentrations will drop quickly, i.e. $c_{\mathrm{met}} \approx 0$, and the relative MetA abundance will decay slowly,

$$\left.\frac{\mathrm{d}\varphi_{\mathrm{MetA}}}{\mathrm{d}t}\right|_{c_{\mathrm{met}}=0} = -\eta\varphi_{\mathrm{MetA}}. \quad \text{(Equation 28)}$$

During this decay, at some point the cell will cross a threshold $\varphi_{\mathrm{MetA}}^{\mathrm{th}}$, below which it cannot recover.

To estimate the dynamics following the nutrient recovery, we first simplify the dynamics of the system. We find that at low methionine concentrations, $c_{\mathrm{met}} \approx 0$, the dynamics of the internal methionine concentration, Equation (1) can be approximated as

$$\left.\frac{\mathrm{d}c_{\mathrm{met}}}{\mathrm{d}t}\right|_{c_{\mathrm{met}}=0} = j_{\mathrm{in}} + h\varphi_{\mathrm{MetA}}. \quad \text{(Equation 29)}$$

Equation (29) means that in the absence of methionine, there is no protein production, no drain to polyamine synthesis and, because there is no growth, there is no dilution. The dynamics is entirely determined by production $h\varphi_{\mathrm{MetA}}$ and import $\tilde{j}_{\mathrm{in}}$. To get an estimate of the timescale of this recovery, we calculate the rate change of methionine production

$$\left.\frac{\mathrm{d}\log c_{\mathrm{met}}}{\mathrm{d}t}\right|_{c_{\mathrm{met}}=0} = \frac{\tilde{j}_{\mathrm{in}} + h\varphi_{\mathrm{MetA}}}{c_{\mathrm{met}}} \gg \frac{\tilde{j}_{\mathrm{in}} + h\varphi_{\mathrm{MetA}}}{c_{\mathrm{met}}^{\mathrm{g}}} \approx 80\ \mathrm{h}^{-1}, \quad \text{(Equation 30)}$$

where we used the upper bound that the methionine concentration c_{met} is lower than the growth steady state $c_{\mathrm{met}}^{\mathrm{g}} = 1.5 \cdot 10^{-4}$ M.

In comparison, the dynamics of the relative MetA abundance at $c_{\mathrm{met}} \approx 0$ is still mostly determined by degradation, as synthesis is small. We thus can estimate the rate change of the relative MetA abundance as

$$\left.\frac{\mathrm{d}\log \varphi_{\mathrm{MetA}}}{\mathrm{d}t}\right|_{c_{\mathrm{met}}=0} = -\eta \approx -1.6\ \mathrm{h}^{-1}, \quad \text{(Equation 31)}$$

When we compare Equation (30) with Equation (31), we see that methionine relaxes much faster than MetA. This common feature of cellular metabolism allows us to separate the dynamics of the system into a fast and slow phase, which we will use in the next section to calculate the unstable fixed-point.

Calculation of the unstable fixed-point

The fact that the timescale of methionine recovery is faster than MetA means that, first, methionine concentration will increase, until consumption of methionine matches production. This is mathematically given by the nullcline $\mathrm{d}c_{\mathrm{met}}/\mathrm{d}t = 0$, Equation (12), at a constant φ_{MetA} that equals the initial condition. Thereafter, both c_{met} and φ_{MetA} will slowly increase or decrease together, until they finally converge to either the growth or dormancy steady state.

Whether they increase or decrease depends on whether the fast phase ends at a position above or below the unstable fixed-point on the methionine nullcline. A cell that started from the threshold $c_{met} = 0$ & φ_{MetA}^{th} will land at the unstable fixed-point, $c_{met} = c_{met}^{unst}$ & $\varphi_{MetA} = \varphi_{MetA}^{unst}$. Because during this phase φ_{MetA} is largely constant, we conclude that the threshold relative abundance of MetA, φ_{MetA}^{th}, is roughly equal to the relative MetA abundance at the unstable fixed point,

$$\varphi_{MetA}^{th} \approx \varphi_{MetA}^{unst}. \quad \text{(Equation 32)}$$

We can calculate the position of the unstable fixed point analogous to the above discussion of the two stable fixed points that led to the conditions of the three stability regimes, Equations 25–27. In the regime around the unstable fixed point, drain has saturated, $u(K_M \ll c_{met}) = 1$. At the same time, c_{met} is still much smaller than at the growth fixed-point, c_{met}^{g}. This regime is given by $K_M \ll c_{met} \ll c_{met}^{g}$. In this case, the methionine nullcline is given by $\varphi_A \approx a_1 c_{met} + a_2 - \tilde{j}_{in}$ and the relative MetA abundance nullcline is given by $\varphi_{MetA} \approx \chi_{MetA} \tilde{\eta}^{-1} c_{met}$. Solving the relative MetA abundance nullcline for c_{met} and inserting it into the methionine nullcline gives us an estimate for the unstable fixed point,

$$\varphi_{MetA}^{unst} = \frac{a_2 - \tilde{j}_{in}}{1 - a_1 \tilde{\eta} \chi_{MetA}^{-1}}, \quad \text{(Equation 33)}$$

or written in the original parameters

$$\varphi_{MetA}^{unst} = \frac{1}{h} \frac{k_d - j_{in}}{1 - h c_{met}^{pro} \eta \chi_{MetA}^{-1}}. \quad \text{(Equation 34)}$$

Equation (34) then defines the growth threshold, because of Equation (32).

Calculation of lag time

In this section, we aim to estimate the lag times of the population. Lag times are caused by the recovery of a small, growing subpopulation. For this reason, we first study the heterogeneity of gene expression that leads to the subpopulations, second, what determines the size of the subpopulations and third, how the size of the subpopulations affects lag time.

Heterogeneity in relative MetA abundance

We investigate how the existence of a threshold can lead to a separation of the population into two growth and dormancy states. Generally, it is known that gene expression is a highly heterogeneous process, due to the stochastic synthesis and degradation of mRNAs and proteins (Friedman et al., 2006; Taniguchi et al., 2010). Phenomenologically, the abundance of proteins such as MetA is well described by a gamma distribution (Friedman et al., 2006; Taniguchi et al., 2010),

$$p(\varphi_{MetA}) = \frac{\varphi_{MetA}^{a-1} \exp\left(-\varphi_{MetA} b^{-1}\right)}{\Gamma(a) b^a}, \quad \text{(Equation 35)}$$

where a is the number of mRNA synthesized per cell cycle and b the number of proteins synthesized per mRNA. Due to the nature of the gamma distribution, a also equals the inverse of the noise, $\sqrt{a}^{-1} = \sigma/\xi$ and b equals the Fano factor, $b = \sigma^2/\xi$, where σ is the standard deviation and $\xi = ab$ is the average. In Table S2, we estimate the average MetA abundance, $6.13 \cdot 10^{-4}$ using ribosome profiling data from 37°C (Li et al., 2014a). At higher temperatures there will be a significant increase in the abundance of misfolded, aggregated or otherwise inactivated MetA. We assume that the abundance of active MetA, φ_{MetA}, during exponential growth remains constant, and that inactivation is compensated by increased MetA expression, see Section D.3 for details. In order to estimate the noise, we take the median noise, $\sqrt{a}_{median}^{-1} = \sigma/\xi_{median}$, of proteins with an average copy number of more than 10 (Taniguchi et al., 2010) and find $\sqrt{a}_{median}^{-1} = 0.4$. We use this value to plot the gamma distribution of MetA in the main text. However, we want to note that neither of these values appear in the theoretical predictions for the exponential scaling of lag time with respect to duration of starvation, calculated further down in Equation (43).

Calculation of lag times

During starvation, the relative abundance of MetA decays exponentially due to thermal inactivation (Mordukhova et al., 2013),

$$\varphi_{MetA}(t) = \varphi_{MetA}(0) \exp(-\eta t), \quad \text{(Equation 36)}$$

and the relative MetA abundance in many cells will falls below the threshold φ_{MetA}^{th} required for growth, calculated in Equation (34). By saying that all cells above the threshold will recover and cells below the threshold will not recover, we implicitly neglect gene expression noise during recovery.

We can calculate the number of recovering cells by integrating the probability distribution, Equation (35), obtained after a starvation time τ, from the growth threshold φ_{MetA}^{th} to infinity,

$$\Pi\left(\varphi_{MetA}^{th}, \tau\right) = \int_{\varphi_{MetA}^{th}}^{\infty} p(\varphi_{MetA}(\tau)) \mathrm{d}\varphi_{MetA}. \quad \text{(Equation 37)}$$

We can estimate the resulting lag time by assuming that recovery of individual cells is fast. Then, lag time will be entirely determined by a growing population Π (growing immediately at growth rate μ) and a dormant population $1 - \Pi$ (that will never grow). These dynamics of the two subpopulations and the resulting lag time is sketched in Figure 3E.

The resulting biomass growth of the population, is given by

$$M(t) = M(0)\left(\left(1 - \Pi\left(\varphi^{\mathrm{th}}_{\mathrm{MetA}}, \tau\right)\right) + \Pi\left(\varphi^{\mathrm{th}}_{\mathrm{MetA}}, \tau\right)\exp(\mu t)\right). \quad \text{(Equation 38)}$$

Note that in this description we are focusing on describing growth, and we are neglecting the slow decay of optical density observed during starvation and lag, see Figure 1.

In order to calculate the lag time, we study the asymptotic growth, when the growing subpopulation has out-grown the non-growing population. In this regime, $\Pi(\varphi^{\mathrm{th}}_{\mathrm{MetA}}, \tau)\exp(\mu t) \gg 1$, and the biomass growth reaches

$$M(t) = M(0)\Pi\left(\varphi^{\mathrm{th}}_{\mathrm{MetA}}, \tau\right)\exp(\mu t) = M(0)\exp\left(\mu\left(t - T_{\mathrm{lag}}\right)\right) \quad \text{(Equation 39)}$$

with the lag time

$$T_{\mathrm{lag}} = \frac{1}{\mu}\ln\left(\frac{1}{\Pi\left(\varphi^{\mathrm{th}}_{\mathrm{MetA}}, \tau\right)}\right). \quad \text{(Equation 40)}$$

Scaling of lag time with physiological parameters

To understand the impact of experimental perturbations we are looking for analytical scaling laws between the measurable output lag time and biological parameters such as MetA pre-expression, starvation time and degradation rate. For this, we note that long lag times are caused by very small growing subpopulations. The growing subpopulation $\Pi(\varphi^{\mathrm{th}}_{\mathrm{MetA}}, \tau)$ becomes small when the threshold $\varphi^{\mathrm{th}}_{\mathrm{MetA}}$ is much larger than the mean of the distribution $p(\varphi_{\mathrm{MetA}}(\tau))$. Thus, the growing subpopulation is represented by the tail of the gamma distribution, which is exponential with relative MetA abundance $\varphi_{\mathrm{MetA}}(t)$ that decreases during starvation, and is given by

$$p(\varphi_{\mathrm{MetA}}) \propto \exp\left(-\varphi_{\mathrm{MetA}}(t)b^{-1}\right). \quad \text{(Equation 41)}$$

We can then obtain the growing subpopulation after a certain starvation time τ using Equation (37),

$$\Pi\left(\varphi^{\mathrm{th}}_{\mathrm{MetA}}, \tau\right) \propto \exp\left(-\varphi^{\mathrm{th}}_{\mathrm{MetA}} b^{-1}\exp(\eta\tau)\right). \quad \text{(Equation 42)}$$

The growing subpopulation thus scales with a

(1) double-exponential form with starvation time τ,
(2) double-exponential form with degradation rate η,
(3) exponentially with the growth threshold $\varphi^{\mathrm{th}}_{\mathrm{MetA}}$,
(4) exponentially with the inverse of the mean pre-expression $\xi = ab$.

By plugging in the growing subpopulation, Equation (42), our derivation of lag time Equation (40), we find that lag time scales proportional to,

$$T_{\mathrm{lag}} \propto \mathrm{const} + \varphi^{\mathrm{th}}_{\mathrm{MetA}} b^{-1}\exp(\eta\tau). \quad \text{(Equation 43)}$$

In summary, lag time scales approximately

(1) exponentially with starvation time τ,
(2) exponentially with degradation rate η,
(3) linearly with the growth threshold $\varphi^{\mathrm{th}}_{\mathrm{MetA}}$,
(4) linearly with the inverse of the mean pre-expression $\xi = ab$.

Estimates of physiological parameters

Using published physiological characterization of E. coli, we can estimate the parameters used in the theory. The results are summarized in Table S2.

Growth physiology

At 45°, *E. coli* in minimal medium supplemented with glycerol has a growth rate of about $\mu^{\mathrm{g}} = 0.45\ \mathrm{h}^{-1}$. The typical cell volume in minimal medium is about $V = 1.3\ \mu\mathrm{m}^3 = 1.3{\cdot}10^{-15}$ l, with a protein mass of about $M = 165$ pg (Neidhardt, 1996). The exact numbers of volume and mass do not matter for the bistability conditions, but serve the purpose to estimate parameters such as the MetA copy number per cell.

Methionine and related compounds

The internal concentration of free methionine (molar mass $m_{\mathrm{met}} = 149\ \mathrm{g\ mol}^{-1}$) in cells growing in minimal medium is about $c^{\mathrm{g}}_{\mathrm{met}} = 150\ \mu\mathrm{M}$ at 37°C (Bennett et al., 2009). Using that the internal methionine concentration is not much different at 45°C, we estimate the proportionality constant between methionine concentration and growth rate, $k_{\mathrm{p}} = \mu^{\mathrm{g}} {c^{\mathrm{g}}_{\mathrm{met}}}^{-1} = 3.0{\cdot}\ 10^3\ \mathrm{M\ h}^{-1}$.

The spermidine concentration, the major polyamine that drains methionine, is $c_{spe} = 1.4$ mM at 37°C (Neidhardt, 1996). The synthesis of each spermidine requires one S-adenosyl-methionine, which is directly draining the methionine pool. The resulting byproduct, S-methyl-thioadenosine cannot be recycled back to methionine without passage through MetA.

While the spermidine pool is 10-fold larger than the free methionine pool, we note that the majority of the methionine is bound inside proteins, where they make up about 3.23% of the protein mass, see Table S2 and Figure S6. This corresponds to a methionine concentration of about. $c_{met}^{pro} = 3.23\% \, M m_{met}^{-1} V^{-1} = 27.5$ mM.

Thus, we conclude that during growth, about 27.5 mM/1.4 mM = 20 fold more methionine goes into protein synthesis than into spermidine synthesis. In terms of systems parameters, this ratio can be written as

$$\frac{k_d}{\mu^g c_{met}^{pro}} = \frac{1}{20}, \qquad \text{(Equation 44)}$$

when we assume that $u(c_{met})$ is saturated at $u(c_{met}) = 1$ at full growth.

Enzymatic parameters of MetA

From the measured copy number of MetA, $N_{MetA} = 1711$ (Li et al., 2014a), measured at 37°C, we estimate the relative abundance of active MetA as $\varphi_{MetA}^{g} = N_{MetA} m_{MetA} M^{-1} N_A^{-1} = 6.13 \cdot 10^{-4}$, where we used the Avogadro number, $N_A = 6.022 \cdot 10^{23} \text{mol}^{-1}$, the typical cell mass $M = 165$ pg, and the molar mass of MetA, $m_{MetA} = 3.56 \cdot 10^4$ g mol^{-1}. In our model, we assume that this active fraction of MetA is independent of temperature, which is based on the assumption that the enzymatic rate of MetA is similar between temperatures and that the expression just enough MetA to sustain growth. The total MetA fraction, which can include also inactive MetA, such as in its aggregated form, will be larger than φ_{MetA}^{g} and will increase with increased inactivation. We do not model the total abundance of MetA and instead focus on the active MetA abundance φ_{MetA}. From this active MetA abundance, we estimate the methionine production rate by MetA, h, as $h = (c_{met} + c_{met}^{pro}) \mu^g / \varphi_{MetA}^{g} = 20.3$ Mh^{-1}.

In order to maintain a given active MetA abundance during growth, the expression level has to compensate for changes in degradation. In our model, this is reflected in the synthesis fraction of MetA, χ_{MetA}, which is defined as the fraction of the total protein mass synthesis directed toward MetA. This synthesis fraction then has to be $\chi_{MetA} = \varphi_{MetA}(\eta + \mu^g)/\mu^g = 2.79 \cdot 10^{-3}$, where we used Equation (S11). The degradation rate of MetA is about $\eta(37°\text{C}) = 1.1$ h^{-1} at 37 °C and increases to $\eta(45°\text{C}) = 1.6$ h^{-1} at 45 °C (Mordukhova et al., 2013). For the growth rate we use $\mu^g = 0.45$ h^{-1}. With this modeling choice, the expression of MetA is increased in response to degradation and inactivation (caused by temperature), such that the fraction of active MetA remains temperature-independent. The upregulation of MetA expression is supported by experimental data (Biran et al., 1995, 2000). The fold-change in expression between no degradation and full degradation at $\eta = 1.6$ h^{-1} estimated by our model, $(\eta + \mu^g)/\mu^g = 4.5$, is roughly consistent with the observed 3.8-fold increase of MetA mRNA expression levels (Biran et al., 1995) and 4.0-fold increase in total MetA (active and inactive) (Biran et al., 2000). Note that we do not model any changes of temperature within this manuscript, and therefore assume that η and χ_{MetA} are constant in all simulations and calculations.

Compound parameters

The above parameters together determine the essential parameters of the system, a_1, a_2, a_3 and $\tilde{\eta}$ that are summarized in Table S2.

QUANTIFICATION AND STATISTICAL ANALYSIS

Quantification of lag time

The lag time after glycerol re-addition was extracted from optical density measurements, and corrected for the loss of viability during the period of starvation. Growth was modeled as $OD_{600} = A + Be^{\mu t}$, which for long times converges to $\lim_{t \to \infty} OD_{600} = Be^{\mu t} = (A + B)e^{\mu(t - T_{lag})}$, with lag time T_{lag}. We extracted growth rate μ and the growing fraction of cells, B, from the time derivative of optical density $\text{d}\, OD_{600}/\text{d}t = \mu B e^{\mu t}$, using a least square fit across the recovery regime where the time derivative increases exponentially. We measure $(A + B)$ as the optical density after dilution. The lag time $T_{lag} = -\mu^{-1} \ln(B/(A + B))$, can then be calculated from the extracted parameters. Lastly, because optical density measurements do not distinguish between living and dead cells in the culture, and a fraction of the culture has perished during starvation, we corrected the lag time estimation by subtracting the number of dead cells N_d from the initial number $N(0) = A + B$. This gives a correction factor $-\mu^{-1} \ln\left(\frac{N(0)}{N_d}\right)$. For 5 h starvation at 45°C, about one third of the cells perish. Thus, with growth rate 0.45/h at 45°C, this yields a correction factor of 0.9 h. In the main text, all lag times are corrected for perished cells. Note that the bi-exponential fits in Figure 1, that include dynamics of both death and growth, are not used to extract lag times.

Survival quantification

Survival in starvation was quantified by counting colony forming units (CFU). Samples were diluted in carbon free N^-C^- minimal medium and spread on LB agar plates using Rattler Plating Beads (Zymo Research, Irvine, CA, USA) with a target density of 200 colonies per plate. LB agar was supplemented with 25 μg/ml 2,3,5-triphenyltetrazolium chloride to stain colonies and increase contrast for automated colony counting (Scan 1200, Interscience, Saint-Nom-la-Bretèche, France). Staining or automation of counting had no significant effect on viability measurements or accuracy, compared to unstained, manually counted samples (<1% systematic error).

Petri dishes were 92 × 16 mm (Sarstedt, Nümbrecht, Germany) and agar plates were incubated for 12 h at 37°C to ensure optimal colony size.

Statistical analysis

Lag times with individual tests, e.g. methionine versus no methionine, were performed in 2–3 biological repeats as mentioned in figure captions and are reported with one standard deviation. Measurements that are quantitative tests, e.g. influence of starvation time, were performed as single repeats, at multiple different perturbation strength. Results of fits are reported with standard error. Measurements of cell survival to antibiotic treatment were performed in duplicates for each temperature. Survival measurements upon temperature shift from 37, 40, 42 and 45 °C to 50°C were performed at least twice for wild-type and MetA stabilized mutants.